UNIVERSITA' DEGLI STUDI DI NAPOLI

"FEDERICO II"

DOTTORATO DI RICERCA IN

NEUROSCIENZE E PATOLOGIA DELL'INVECCHIAMENTO CEREBRALE

XVII CICLO

QUANTIFICATION OF CEREBRAL TISSUE VOLUMES IN MULTIPLE SCLEROSIS: GLOBAL AND REGIONAL ANALYSIS

COORDINATORE:

Chiar.mo PROF. LUCIO ANNUNZIATO

DOTTORANDA:

ING. ANNA PRINSTER

ANNO ACCADEMICO 2004-2005

ABBREVIATIONS

MS	Multiple Sclerosis
MRI	Magnetic Resonance Imaging
MR	Magnetic Resonance
GM	Gray matter
WM	total White matter
aWM	abnormal White matter
CSF	Cerebrospinal Fluid
fGM	fractional Gray matter (GM/ICV)
fWM	total fractional White matter (WM/ICV)
faWM	fractional abnormal White matter (aWM/ICV)
fCSF	fractional Cerebrospinal Fluid (CSF/ICV)
ICV	Intracranial volume
LL	Lesion Load
RR	Relapsing Remitting
PP	Primary Progressive
SP	Secondary Progressive
PD, N(H)	Proton Density
TE	echo time
TR	repetition time
QMCI	Quantitative Magnetic Color Imaging
ROI	Region of Interest
PAWM	Potentially abnormal WM
PL	potential lesions
VBM	Voxel-Based Morphometry
EDSS	Expanded Disability Status Scale
DD	Disease Duration
CI	Confidence Interval
FWHM	Full Width at Half Maximum

INDEX

INTRODUCTION

Multiple sclerosis (MS) is the most common neurological disease of young adults, and despite the fact that the disease was described over 130 years ago, understanding of pathogenesis remain elusive. The histopathologic features of MS include multiple foci of inflammation and demyelination as well as potentially substantial destructive or degenerative changes in both white matter (WM) and gray matter (GM) (Cifelli, 2002; Kidd, 1999; Peterson, 2001; Trapp, 1998). In the last 15 years, Magnetic Resonance Imaging (MRI) has assumed an important role as a tool to assist in the diagnosis of multiple sclerosis and to monitor the evolving disease *in vivo.* MRI allows to identify with high specificity white matter lesions, providing a sensitive measure of the evolving pathology, which is often not clinically apparent.

Abnormalities have been reported also in the so-called normal appearing white matter and cortex using quantitative magnetic resonance methods, and pathological studies have confirmed the presence of disease in these regions. Furthermore, MRI data have led to the hypothesis that progression of the disease, up to a stage of no return, is dependent on the cumulative effect of axonal damage (De Stefano, 2001), which may ultimately result in MRI-visible brain atrophy (Miller, 2002).

Tissue damage in MS is in fact not limited to the white matter (WM) as from inflammation axonal transection ensues (Ferguson, 1997; Trapp, 1998), and this process may extend by Wallerian degeneration, indirectly demonstrated by N-

acetylaspartate reduction in MR spectroscopy studies (Davie, 1995; Davie, 1994; Rooney, 1997), possibly contributing to gray matter (GM) loss.

Progression of brain atrophy, above normal age-related brain volume changes, has been detected in MS using linear measures of width of the ventricles and/or volumetric measures of the brain/intracranial volume (ICV) ratio (Adams and Koziol, 2000; Losseff, 1996; Rudick, 1999; Simon, 1999), over a period of time as short as 1 year. These findings raised the hypothesis that neurodegenerative pathology in MS may represent a major part in the development of permanent disability. Moreover the accumulation of damage to the nervous system may play a different role in the different clinical types of MS: relapsing-remitting (RR), primary progressive (PP), secondary progressive (SP).

Consequently, there has been a growing interest on the possibilities offered by MRI to measure structural changes in the brain of MS patients, particularly regarding techniques which provide quantitative estimates of brain tissue volumes.

QUANTIFICATION OF BRAIN TISSUE VOLUMES WITH MRI: SEGMENTATION TECHNIQUES

There has been an active search for sensitive MRI methods to measure brain atrophy and other objective parameters of tissue damage. In an effort to obtain reliable, reproducible, and objective measurements of brain atrophy, MRI methods have evolved from semiautomated, operator-dependent segmentation techniques to automated, operator-independent ones (Miller, 2002; Pelletier, 2004).

Quantification of brain tissue volumes involves the identification of each intracranial tissue, including GM, WM, CSF. Such object-based processes may involve some or all of the following: detecting the presence of the tissues, localizing their boundary or the position of their centre, measuring their size, characterizing their shape and identifying their anatomical name or pathological type.

These processes all depend on the fundamental underlying process of segmentation, that in a more general sense can be defined as the partitioning of the image into objects. Segmentation methods need to be reproducible, accurate and efficient.

Segmenting a brain to divide it into regions usually involves examining every voxel in the image and assigning it a label that associates it with a tissue. The assignment can be based on properties of that voxel, properties of its neighbours, and/or similarity to other voxels which are already assigned to a region.

In medical images of the brain, the regions are usually referred to by experts with anatomical names for specific objects (such as “thalamus”) or with a names for a type of tissue, vis. gray matter (GM), white matter (WM), or cerebrospinal fluid (CSF). Structures are mainly recognized from their morphology and spatial relationships. Many of the individual structures are composed of one class of tissue. Various parameters of the segmented structures can be calculated, and compared with normal structures or previous measurements performed using the same technique. MR image segmentation allows the visualization of the individual anatomical structures in 3D, providing an aid to surgery and treatment planning, as well as a means for studying the effect of the locality of abnormal tissues in disease.

In general, segmentation and labelling of MR images is a very difficult and time-consuming process (Farmer, 1996; Kapur, 1995). Often there is not enough information in the image to segment a complete structure. Low quality of data and having irregular shape which is difficult to represent mathematically makes MR segmentation more difficult.

MR data characteristics

Before focusing on segmentation techniques, it is worth to take a look to some characteristic of MR data that affect image segmentation: noise, partial volume effect, radio-frequency inhomogeneities and motion.

1. Noise

The signal to noise ratio can be relatively low for poor quality MR images. The commonly used techniques for image noise reduction involve some form of smoothing. Smoothing modifies each pixel intensity according to the intensities of its spatial neighbors. While reducing the noise, these techniques also reduce the image contrast. There are also other noise reduction techniques that make a priori assumptions about the statistical nature of the noise. Noise is a frequent problem in any image acquisition process, including MRI. In many cases segmentation techniques are evaluated on their relative sensitivity to noise.

2. Partial Volume Effect

MR images have limited spatial resolution, thus, each voxel can be occupied by more than one tissue type; its intensity can be the average of the intensity from all component tissues, which blurs the intensity distinction between tissue classes at the boundary of the objects. This effect blurs many of the tissue boundaries of an MR image, making tissue boundary detection difficult (Laidlaw, 1998). Furthermore MR images are usually acquired as a sequence of 2D slices, which are then stacked to form the image of a volume. In-plane spatial resolution is typically higher than the slice thickness, leading to voxels which have cuboidal shape rather than cubic. This anisotropic sampling can cause problems for certain types of segmentation algorithm.

3. Intensity Inhomogeneity

MR images are subject to artefactual variation in signal intensity across the field of view. The main causes are inhomogeneity of the radio-frequency field resulting in non-linear gain artifact in the images. This is problematic for brain segmentation algorithms that assume that voxels containing a particular tissue type have similar intensities throughout the MR volume. The artefactual intensity variation perturbs the intensity distributions, increasing overlap and leading to substantial misclassification when methods based only on intensity are used. Methods to compensate for intensity inhomogeneity are thus important to improve the results of many segmentation algorithms.

4. Motion

Patient movement during the scan causes artefacts. Because signal acquisition occurs in the frequency domain, artefacts in the image space tend to have a complex appearance and are hard to correct by post-processing. The problem is more acute when multimodal datasets are acquired because the duration of image acquisition is usually longer.

Segmentation methods

Separating brain tissues can be done basically in two ways: based on the homogeneity of a region with the so-called region based methods, or if homogeneity is poor but contrast between regions is high with the so-called boundary based methods.

Region based techniques rely on the homogeneity of spatially localized features, whereas boundary based techniques attempt to identify the locations of significant changes in grey level, using discontinuity measures.

Apart from the calculation algorithm used, another important characteristic of the segmentation methods is their operator dependence that goes from manual parcellation through semi-automated to completely automatic operator independent ones.

1. Automatic thresholding

Thresholding is the simplest region-based method, where the similarity criterion is set by the threshold. It is one of the most commonly use image segmentation processes.

The automatic thresholding techniques usually involve four basic steps:

1) A histogram of the MRI voxel intensities is produced
2) A threshold is selected based on the fact that most of the relatively high intensity voxels in the MR image belong to the brain
3) The threshold is then applied to the image to produce a binary mask
4) Some kind of morphology and/or expert knowledge is applied to the binary mask to remove non-brain regions. The resulting mask identifies the brain and thus, the intracranial boundary.

This procedure is usually applied to the histogram of the whole image (global thresholding), but can be performed also locally on any sub-region.

Some authors use iterative thresholding to distinguish brain tissues from others in axial MR slices by means of an adaptive technique, that iteratively adjust the

initial threshold on the basis of the geometry of resulting masks (i.e. the head mask includes the brain mask) (Suzuki and Toriwaki, 1991). This method is ineffective in the presence of RF inhomogeneity and in slices where the brain is not one homogeneous region closely surrounded by the skull (e.g. in the lowermost slices where cerebellum and temporal tips are separated).

Automatic thresholding (Atkins and Mackiewich, 1998; Brummer, 1993) is often used to perform a crude segmentation of the brain. Refinement of the brain contour is then performed using several approaches, including discontinuity-based morphological processing (Atkins and Mackiewich, 1998), active contour and deformable models (Kaus, 2003; Vaillant and Davatzikos, 1997), and other techniques (Chakraborty, 1994; Holden, 1995).

2. Region growing

Region growing methods require the identification of a seed point to start classification of voxel intensity and absorb neighbouring points satisfying a homogeneity measure to expand the region. For this region they are in general semi_automatic method.

The homogeneity measure is computed based on some statistics from region and/or its local neighbourhood. Pannizzo et al. (Pannizzo, 1992) consider the grey level change along horizontal line outward from the centre of the image (brain) to detect intracranial boundary. They use an adaptive threshold to detect the first significant change in the intensity. A running average of voxels along the line is used to refine the boundary.

Zijdenbos et al. (Zijdenbos, 1994) fitted a surface to the voxels initially labelled as a boundary. They then calculated a new threshold and refined the boundary position by applying this threshold.

Hojjatoleslami et al. (Hojjatoleslami and Kruggel, 2001) developed a region growing algorithm which starts from a high grey level point inside the white matter, absorbs the highest grey level point in its boundary to expand the region. A discontinuity measure, so called peripheral contrast, is employed to choose the boundary for the region. Peripheral contrast computes the difference between average grey level of internal boundary and the external boundary during the growing process. It computes a global measure of discontinuity for the boundary of the region which is robust in the presence of noise. The algorithm is used in two steps; in the first step, a starting point inside the scalp is used to segment the scalp and eyes, in the second step the algorithm starts from a seed point inside the white matter to segment brain tissues (WM, GM and CSF). These two starting points are the only interactive settings used.

3. Matching to a normalized template (atlas)

Atlases have been used as a reference for segmentation of 3D MR images by some researchers. This is accomplished by first registering an atlas volume with the subject volume and then using the atlas to segment the mapped structures from the test image. The initial segmentation is then normally refined using various local properties (Dawant, 1999; Hartmann, 1999; Van Leemput, 2001ì).

Many different algorithms for registering the 3D atlas onto the MR volume have been used. An example is described by Hartmann (Hartmann, 1999) who used a two-step registration.

4. Edge detection

Edge detection methods rely on changes in the grey level, rather than their actual values, to produce closed boundary contours. Edges can be detected using a variety of operators including Sobel, Laplace, Perwitt or Canny operators (Mohamed, 1999). Prior smoothing with a Gaussian function, is often used. These operators are generally a type of gradient magnitude transform, the result of which is then thresholded to produce a large number of disconnected edge segments. The disadvantages include the loss of edge detail in certain parts of the image, where magnitude of the edge strength is lower than the global threshold; and the fact that the edge segments are disconnected and must be linked to each other before any objects are extracted.

Among Edge-detection method watershed algorithms are commonly applied to a gradient magnitude image, to divide the image into the small regions with closed boundaries, surrounding a single local minimum of magnitude. Letterboer et al. (Letteboer, 2004) applied the watershed method to anisotropically filtered MR images. They evaluated a range of such operators for the purpose of interactive multi-scale segmentation of grey and white matter in T1 weighted 2D MR images. Along the watershed boundaries, the gradient magnitude is locally maximal in the

direction orthogonal to the edge. The main disadvantage is that when the level of noise is high, a large number of small regions is generated. It is almost always necessary to simplify the watershed segmentation by merging locally similar regions.

5. Active Contour models

Deformable models have been a popular technique for segmentation of medical data, in part because of their ability to incorporate approximate shape constraints. In 3D systems that use such models typically represent anatomical structures using stacks of deformable contours in 2D or may use a true 3D deformable surfaces. Example systems include Chakraborty's Fourier snakes (Chakraborty, 1994).

Atkins (Atkins and Mackiewich, 1998) used an active contour model to refine the boundary between the brain and intracranial cavity. They use a four-term energy function including curvature (to force the contour towards a circular shape), balloon (to push the contour outward to cover a larger region) intensity (to drive the contour toward low intensity area) and gradient (to force the contour toward strong gradient points). The weighted sum of the energy functions is computed and every boundary point is moved to the point of minimum energy in its local neighbourhood.

Chakraborty et al. (Chakraborty, 1994) combined a region-based method to provide an initial segmentation of the image, and then fit a parametrically deformable shape model to find the boundary of interesting features in the

segmented image. Ranganath (Ranganath, 1995) used a snake algorithm to extract the contour from cardiac MRI studies by propagating the snake to sequence of images, with an intermediate processing step. The intermediate process prevents the snake contour from becoming trapped in local minima. The initial contour is crucial step in the snake algorithm.

6. Multiparametric methods

Some groups use multiple sets of MRI volumes to have more information on the images. For example Jackson and colleagues (Jackson, 1993) described a method which segmented the T2 and PD (2-dimensional) histogram into five classes corresponding to GM, WM, CSF MS lesions and other tissues using a cluster algorithm. An ellipse enclosing the two standard deviation confidence limits was calculated and other parameters of the cluster were derived. The ellipse could be extended or reduced interactively on the scatter plot, while viewing the image. Pixels thus classified were displayed in image space.

A system described by Mitchell and colleagues (Mitchell, 1994) was similar to that of Jackson et al. but apparently allowed more interactions. Mitchell's parameterization of the feature space clusters allowed a location in feature space to have graded (fuzzy) membership of a cluster, and also to belong to more than one cluster. This in turn meant that any pixels in the image having the (multispectral) intensity properties of a particular feature space location would also have the same (multi-tissue) fuzzy membership.

Zijdenbos et al. (Zijdenbos, 1994) developed a method which used T1 as well as T2 and PD data sets. For forming feature space clusters, the user input a set of

training points. A neural network algorithm constructed the clusters. They showed that correction for intensity inhomogeneity had a profound effect on the results.

Johnston et al. (Johnston, 1996) acquired dual echo (PD and T2 weighted) and discussed the extent of overlapping intensities of the important tissue classes, but they carried out initial segmentation using the intensity histogram of each echo separately. Class membership was expressed as a probability or fuzzy value, as with Mitchell et al. and Zijdenbos et al. Like other authors, they demonstrated the importance of correction for intensity inhomogeneity. Kamber et al. (Kamber, 1995) registered MS patient scans with a probabilistic anatomical atlas. This was then used to guide the lesion segmentation process with a reported high degree of agreement with manual segmentations.

Udupa et al. (Udupa, 1997) have developed an approach to segmentation which they term "fuzzy-connectedness" and have applied this to the MS lesion quantification on dual echo MR images. The background is masked by applying a threshold which is derived by identifying border voxels in a whole-image histogram of gradient magnitudes. Intensity inhomogeneity is corrected by fitting a second order polynomial to a roughly segmented "CSF object". This is extracted by creating an image from the ratio of T2 and PD values which minimises the pre-correction intensity inhomogeneities. They then use an empirical approach to derive parameters from the 2D histogram for the "fuzzy connectedness" analysis of white and grey matter. In this application, fuzzy connectedness is an index of intensity similarity between two voxels. This "similarity" is a complex function which is high if the mean intensity of the two

voxels is close to a neighbourhood mean, but is reduced if the difference between the intensities of the two voxels is close to a neighbourhood mean of differences. Fuzzy connected objects are then created by linking voxels which are similar to their neighbours; boundaries occur where there are low similarities (i.e. marked differences in intensity) which cannot be circumvented.

Among the multiparametric systems is also included a more recently published method based on the calculation of relaxation properties of each brain voxel, based on signal intensities of MR conventional Spin echo images (T1-w, T2-w and PD-w) which allows to recognize and segment both normal brain tissues and MS lesions (Alfano, 1997; Alfano, 2000).

As this method was the basis for the present work, it is described more in detail hereinafter in its original implementation. Ameliorations introduced for the purposes of the present work are then described (see below section on the first aim of the study).

A MULTIPARAMETRICAL FULLY AUTOMATED SEGMENTATION METHOD FOR MS

Alfano et al. (Alfano, 2000) developed a fully automated segmentation method that included the identification and volume measurement of demyelinated white matter.

The method is based a relaxometric characterization of brain tissues using calculated R1 (= 1/T1), R2 (= 1/T2) and proton density [N(H)] maps from spin-echo MR acquisition sequences. The assessment of MS lesion distribution in the R1, R2, N(H) space indicated that MS lesion classification using the above procedure would require utilization of both relaxometric and geometric features of MS lesions for their classification (14).

Generation of the multiparametric maps

The Alfano's multiparametric approach requires two sets of slices covering the whole brain obtained at 1 or 1.5 T MRI scanner, sampling the whole brain contiguously (Fig. 1). Each set includes conventional spin-echo sequences providing T1w and PD/T2w axial images.

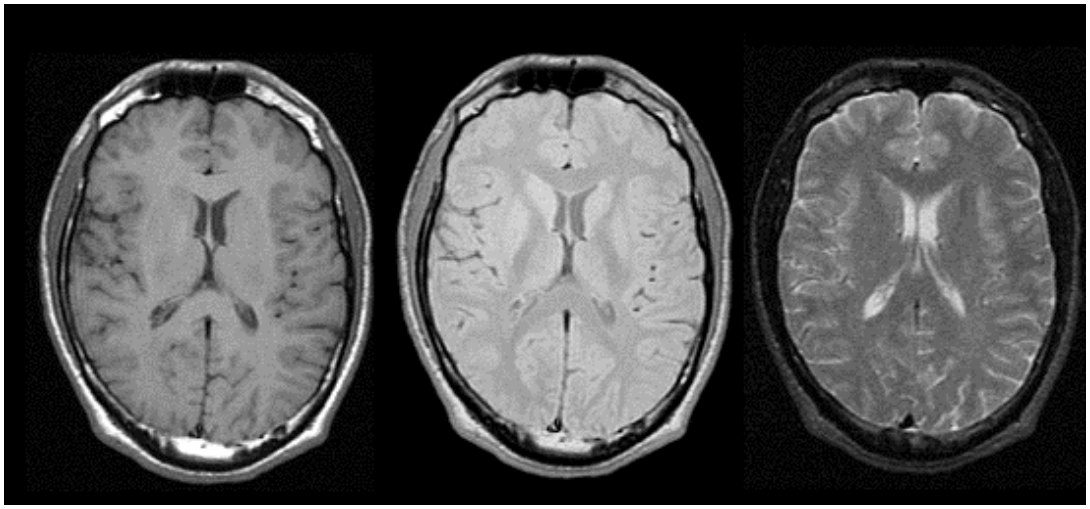

Fig.1

The example of one axial slice from the MRI acquisition is displayed showing the contrast obtained from the spin-echo sequences. Images represent respectively: T1-weighted on the left, PD-weighted in the middle and T2-weighted on the right.

For each slice, relaxation-rate (R1 and R2) and proton-density [N(H)] maps are computed according to the following equations:

$$S = K \bullet N(H) \bullet \frac{1 - 2e^{-(TR - TE/2)R1} + e^{-TR \cdot R1}}{1 + e^{-TR(R2+R1)}} \bullet e^{-TE \cdot R2} \quad [1]$$

$$S = K \bullet N(H) \bullet \frac{1 - 2e^{-[TR - (TE_1 + TE_2)/2]R1} + 2e^{-(TR - TE_1/2)R1} - e^{-TR \cdot R1}}{1 + e^{-TR(R2+R1)}} \bullet e^{-TE \cdot R2} \quad [2]$$

where S is MR signal intensity, N(H) is proton density, K is a constant depending on total device performance and gain, R_1 and R_2 are spin-lattice and spin-spin relaxation rates, respectively (with TE_1 and TE_2 indicating respectively the first and the second echo times of the double-echo sequences). Eqs. [1] and [2],

respectively valid in the transverse steady state for single-echo and double-echo sequences, were derived from the analysis of Bakker and colleagues (Bakker, 1984).

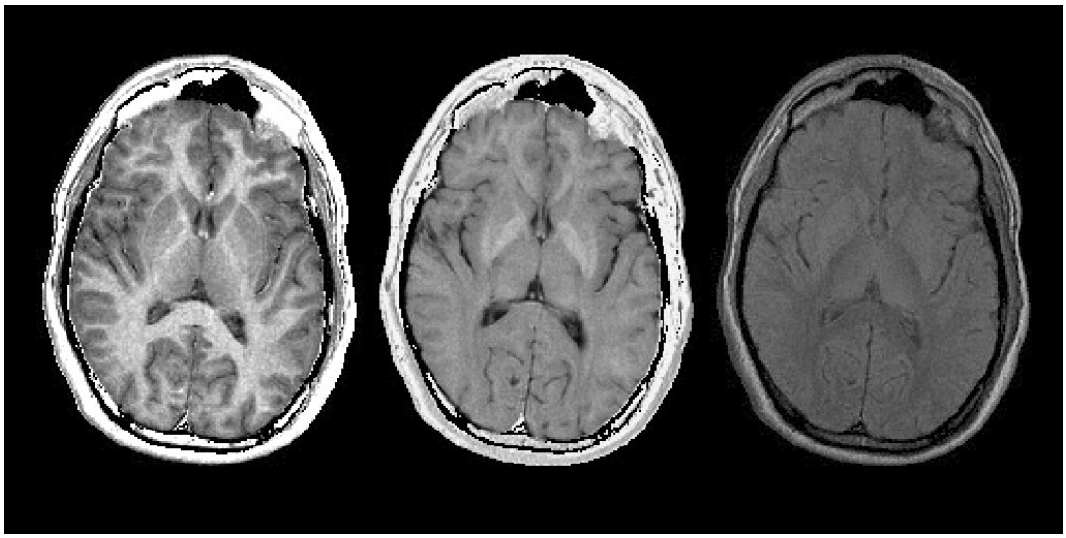

Fig. 2

The example of the three maps derived from the triplet acquisition images of one axial slice according to the formulas [1] e [2]. Images represent respectively: R1 on the left, R2 in the middle and N(H) on the right.

The three maps can be visualized in one color picture by driving the Red, Green and Blue channel with the R1, R2 and N(H) values respectively. The resulting so-called QMCI (Quantitative Magnetic Color Imaging) is shown in Fig. 3.

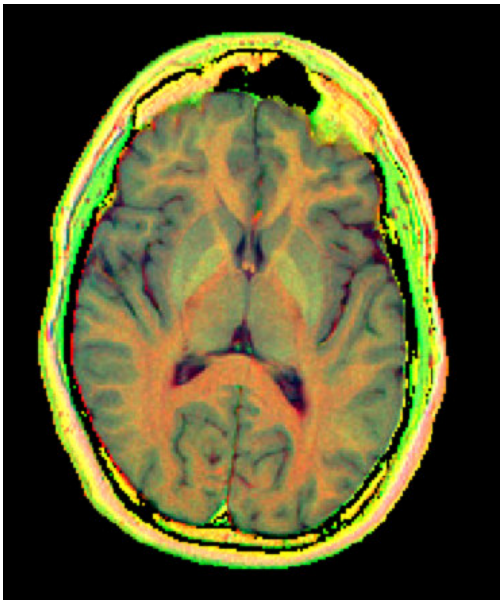

Fig.3

QMCI image of a representative axial slice.

Segmentation procedure

After being calculated for the whole brain volume, the R1, R2 and N(H) values for each voxels of the volume are plotted in a three-dimensional space to identify clusters of voxels belonging to different brain tissues. Fig.4 presents the cluster distribution of the total brain volume in a normal subject, in which the high frequency components were eliminated to better identify clusters of different brain tissues.

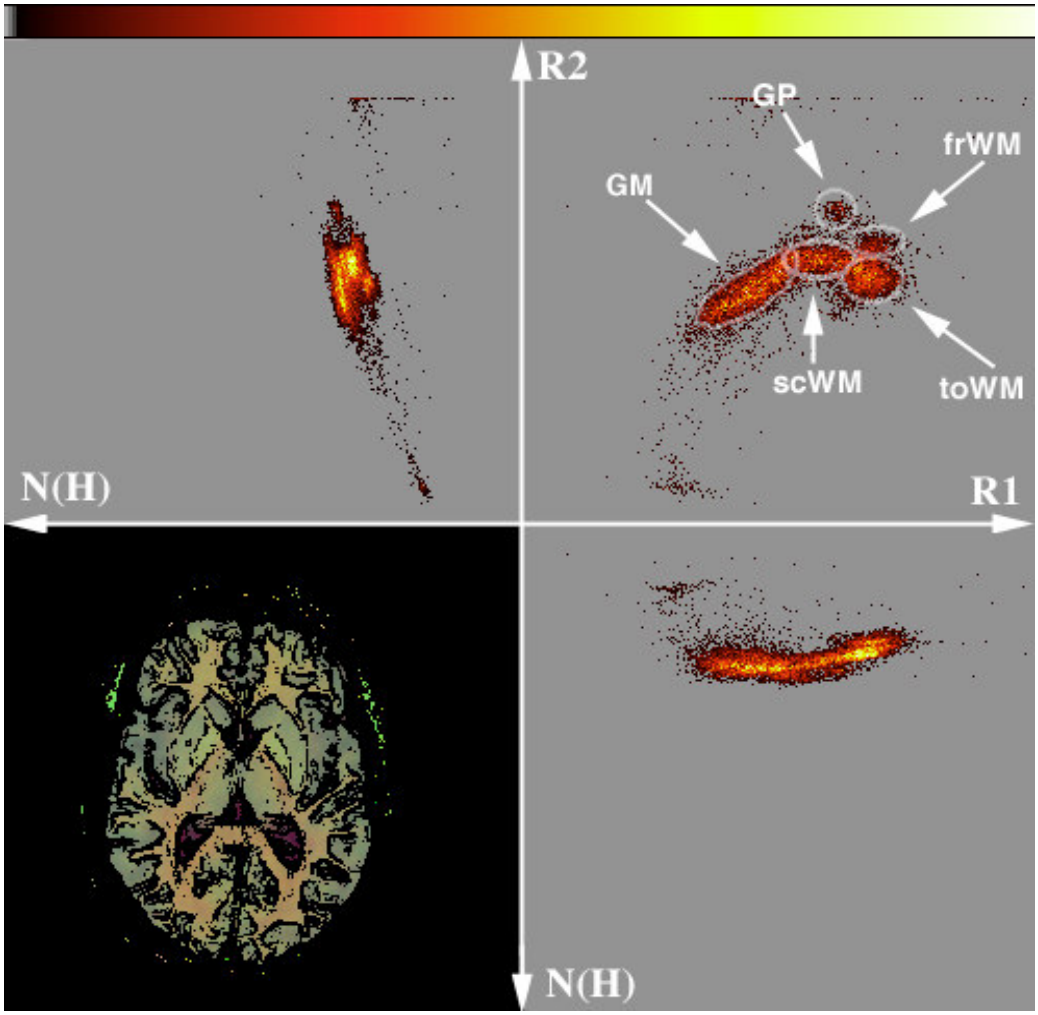

Fig. 4
Voxel distribution in the R1-R2-N(H) space of a whole brain volume form a normal volunteer and a representative QMCI axial slice. The filtering of the high spatial frequency of the image allows to better identify clusters of different tissue types: WM (white matter), GM (gray matter), GP (globus pallidus), frWM (frontal WM), toWM (temporo-occipital WM), scWM (subcortical WM).

Clusters were interactively defined by expert observers with simultaneous comparative assessment of the original signal-intensity MR images, of the segmented images and of the cluster distributions. The resulting ROI boxes, as published (Alfano, 1997) are reported in Fig.5.

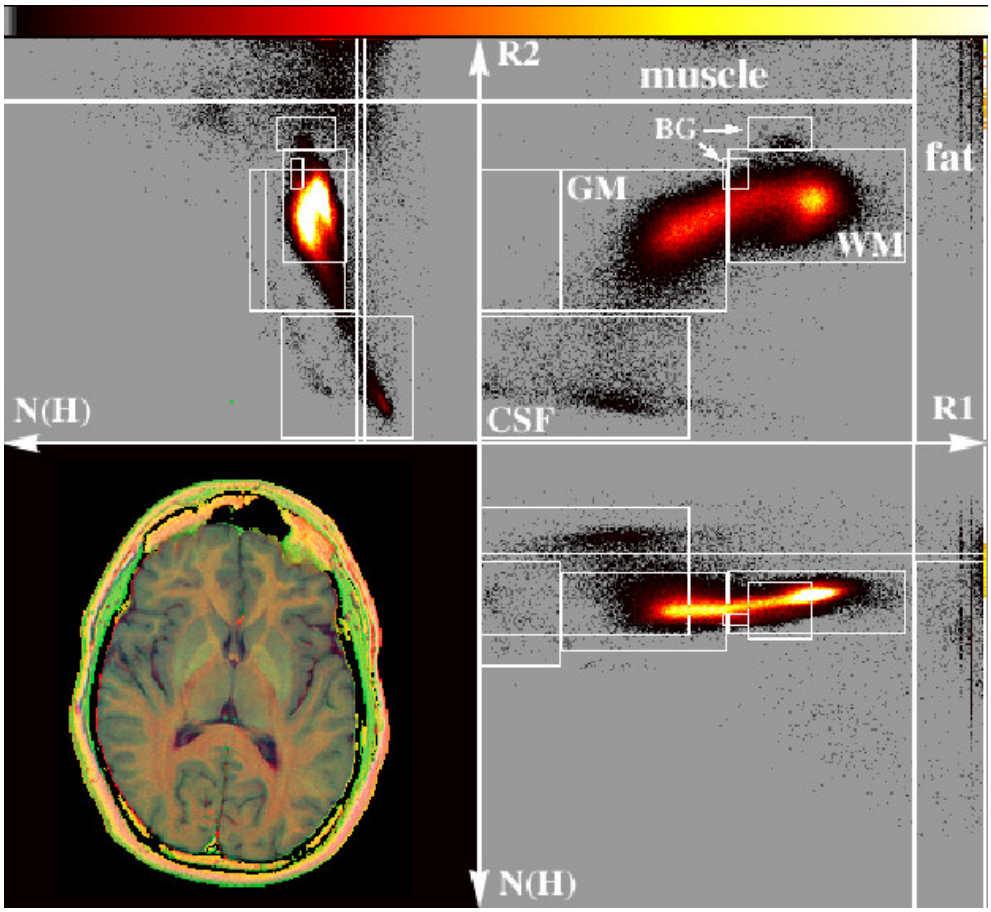

Fig. 5

Voxel distribution in the R1-R2-N(H) space of a whole brain volume from a normal volunteer and a representative QMCI image (lower left). Color scale (top) indicates voxel density. ROIs indicated on the R1-R2 plane identifies different brain tissues.

It is evident from Fig.5 that a crucial step in ROI definition is the separation of the GM and WM clusters, whereas the CSF cluster seemed to be clearly distinct from the other two. The automated procedure for segmentation and volume measurements is based on the following steps: (a) preprocessing of the

multispectral QMCI images; (b) correction for RF inhomogeneities; (c) calculation of GM/WM R2 cutoff and ROI coordinate updating; (d) creation of a preliminary 3D segmentation matrix; (e) elimination of the voxels belonging to extrameningeal tissues, which may fall in one of the cerebral tissue clusters; (f) classification of the remaining voxels; (g) volume calculation and display of the segmented images. The result of the segmentation algorithm with the classification of each voxel of the brain volume is depicted in Fig. 6.

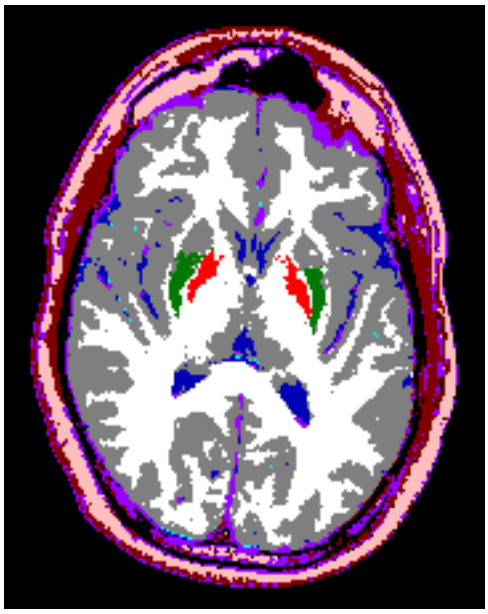

Fig. 6 An axial slice showing an example of the output of the segmentation program. Color coding for segmented images is: GM, gray; WM, white; CSF, blue; putamen, green; globus pallidus, bright red; muscle, dark red; low N(H) tissues, violet; fat, pink.

1. Calculation of GM/WM R_1 cutoff

The algorithm in its published version included a calculation of the GM/WM R_1 cutoff that we modified in the present version of the program as described later on. An adjustment of the GM/WM R_1 cutoff is necessary, because the separation of the GM and WM clusters is critically dependent upon their R_1 values. Therefore the sum of the R_1 histogram for all the slices of the study is obtained and smoothed. The two R1 values corresponding to 10% of the maximum of the histogram ("feet" of the distribution) are determined as shown in Fig. 7. The

GM/WM R1 cutoff value is set at 43% of the distance between the two feet. Such value provided the best GM/WM separation in the segmented images in a test population of 10 normal subjects (age range: 24 to 57 years) originally used to define the position of the normal brain tissue clusters in the multispectral R_1, R_2 and N(H) space. The use of a predefined percentage of the distance between the edges of each distribution from prefiltered data results in a R1 cutoff value tailored to each subjects.

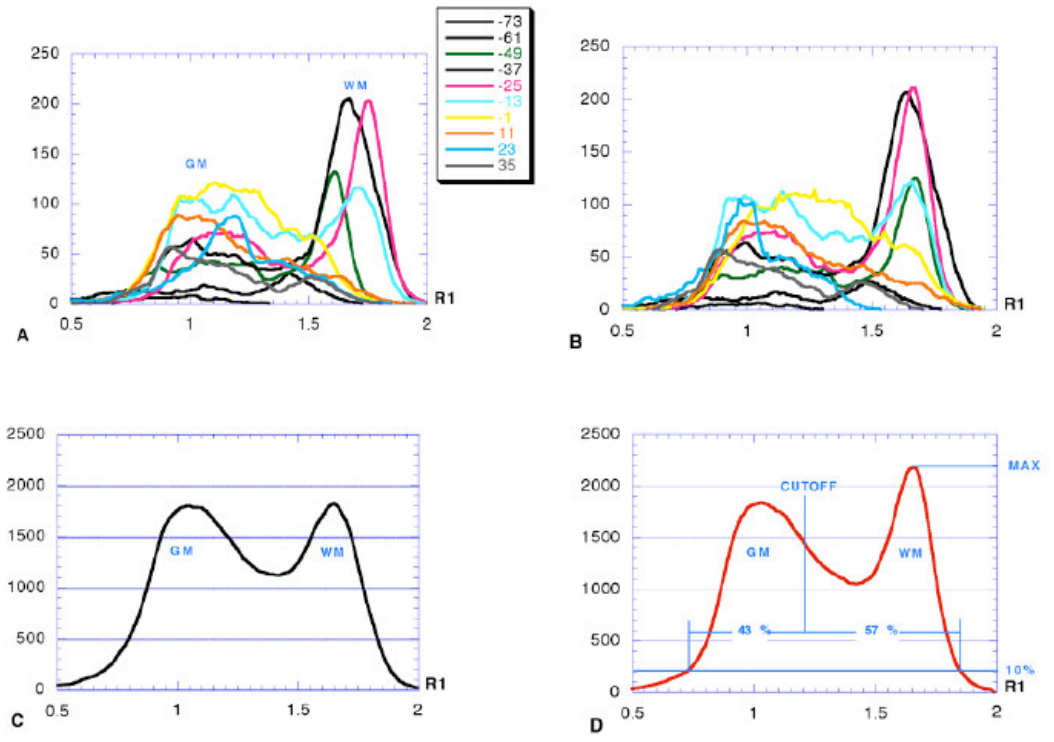

Fig. 7

Volume study performed in a 28-year-old normal subject: distribution along the R1 axis of voxels belonging to GM and WM ROIs in series of representative slices before (A) and after realignment (B) and corresponding sum of all histograms before (C) and after realignment (D). Legend between A and B indicates slice positions (Z axis offset in mm, cranial-caudal direction).

After determining the ROIs positions in R1-R2-N(H) space that allow to assign each voxel to a specific brain tissue based on the test population, the segmentation

procedure was applied to a population of a 50 normal subjects to find age correlation of fraction tissue volumes (fGM, fWM and fCSF normalized for the total intracranial volume obtained from the sum of GM, WM and CSF).

MS plaques automatic segmentation

The Alfano's segmentation method has been successfully applied to the segmentation of MRI studies from MS patients including in the software the automated identification and volume measurements of demyelinated white matter. The assessment of MS lesion distribution in the R1, R2, N(H) space indicated (Fig. 8, 9) that MS lesion classification using the previously described procedure would require utilization of both relaxometric and geometric features of MS lesions for their classification.

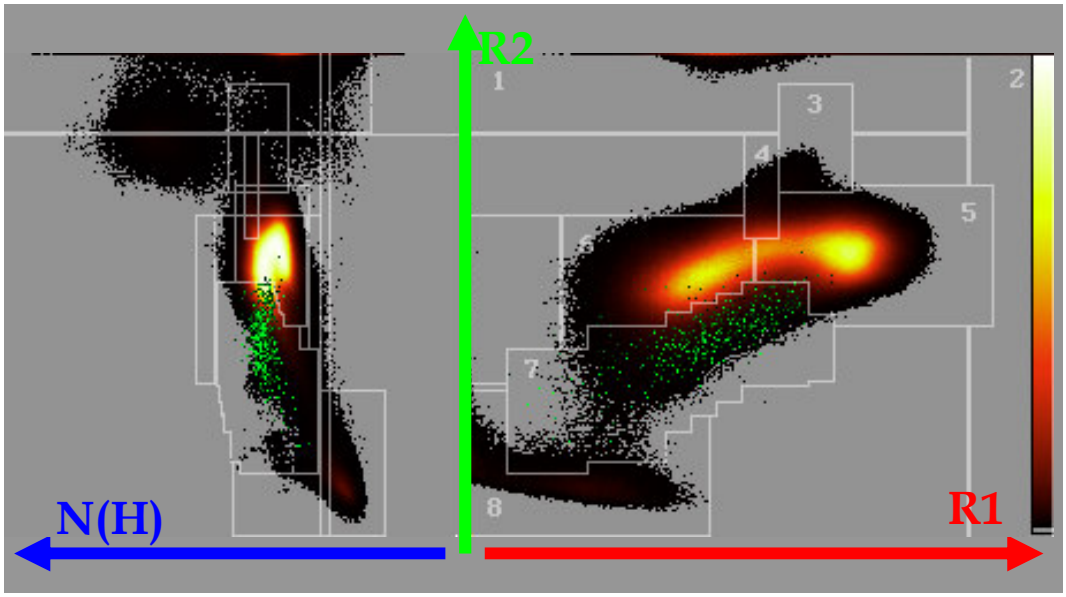

Fig. 8

Projection of the 3D histogram of brain voxels from the 22 MR studies in normal subjects onto the N(H)-R2 (left) and R1-R2 (right) planes. Color scale (right) indicates voxel density. Mean values of the plaques from 18 studies in MS patients are superimposed (green dots; intensity is proportional to plaque volumes). ROIs indicate respectively: 1, muscle; 2, fat; 3, globus pallidus; 4, putamen; 5, white matter; 6, gray matter; 7, potentially abnormal white matter; 8, CSF.

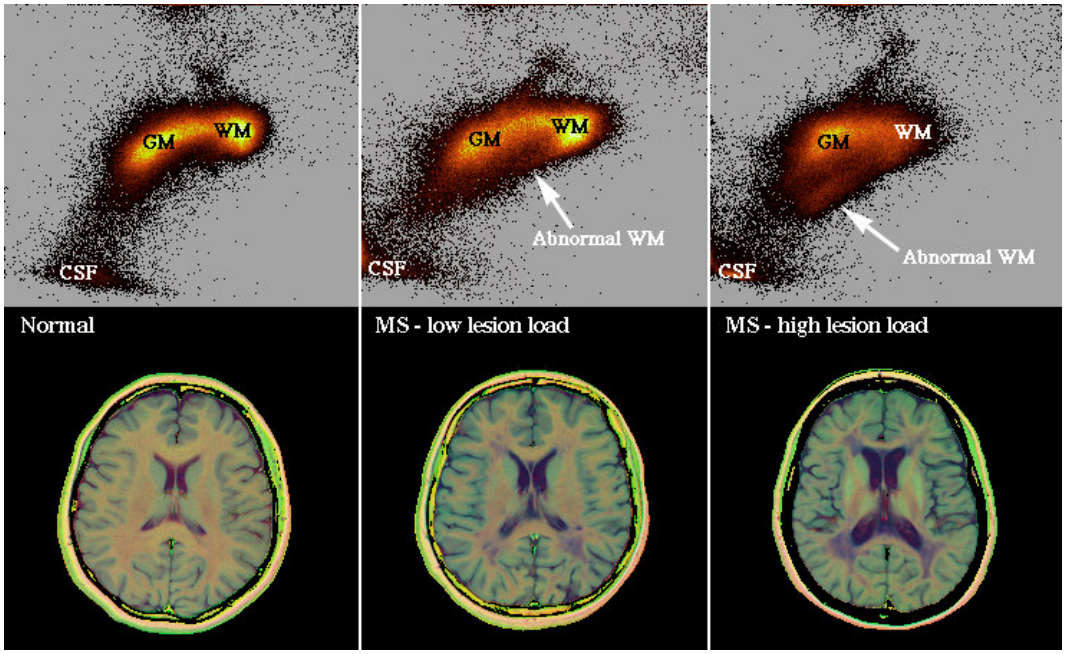

Fig. 9

Projection of the 3D histogram of brain voxels onto R1-R2 plane (upper row) and QMCI maps at the level of the lateral ventricles (lower row) in a normal subject (left) and in two patients with different lesion load. WM 5 white matter, GM 5 gray matter, CSF 5 cerebrospinal fluid. In the two patients different degrees of the involvement of periventricular and subcortical WM (dark violet areas) are shown. The corresponding R1-R2 distributions show the position of abnormal WM.

1. Identification of WM lesions

Figure 10 shows a flow chart of the procedures for the classification of WM lesions.

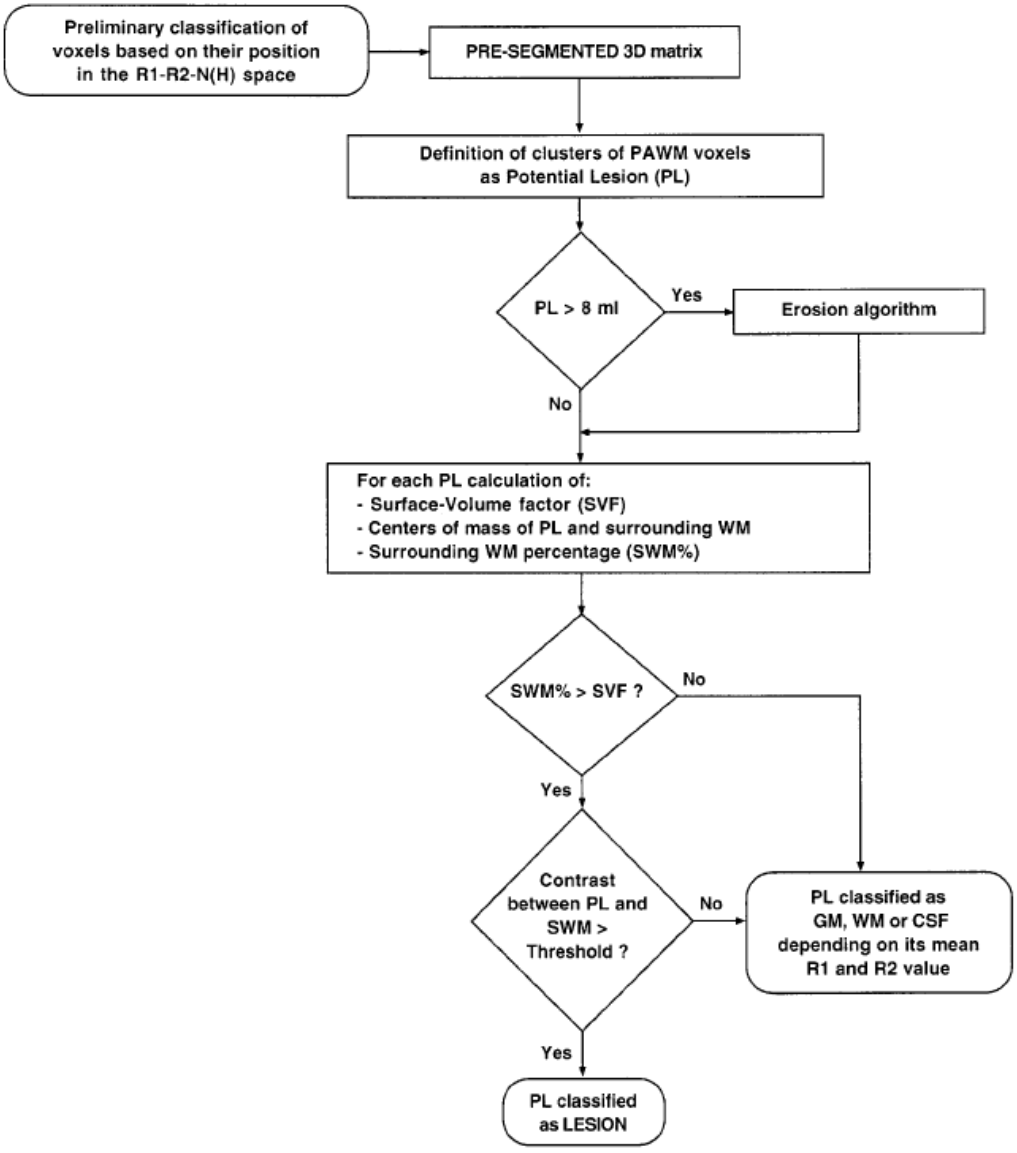

Fig. 10

Flow chart of the procedure for the classification of WM lesions.

The classification of normal brain tissues is based on their distribution in the R1, R2, N(H) multifeature space, where the clusters of GM, WM, and CSF are well defined (Fig. 8, 9). To know the position of the cluster representing the demyelinated WM in the multifeature space, a preliminary analysis was performed on 18 MR studies in 18 subjects with MS. Three neuroradiologists with more than 4 years of experience in brain MRI interpretation, selected WM lesions

on original films [T1-, T2-, N(H)-weighted images] in the MS patients. Neuroradiologists were asked to identify lesions according to conventional diagnostic criteria. A subset of 253 MS lesions (representative of the whole spectrum of MR appearance), identified by at least two observers, were then outlined on the QMCI slices, using an interactive region growing routine written by the authors using Interactive Data Language (Research System, Boulder, CO). For each lesion, the mean value of R1, R2, and N(H) were calculated and superimposed onto a reference distribution of normal intracranial tissues obtained by averaging 22 normal studies (Fig. 8).

In the multifeature space, abnormal WM voxels cover a wide range of R1, R2 values (Fig. 8) and seem to originate from the normal WM cluster and migrate toward lower R1, R2 values. This is more clearly shown when comparing R1, R2 distributions of normal subject with patients with a different lesion load (Fig. 9). Since in the multifeature space the MS lesions partially overlap the normal tissue distribution (Figs. 8, 9), voxel position alone does not allow unequivocal classification of MS lesions but only permits the definition of a ROI for tissues that can be classified as "potentially abnormal white matter" (PAWM). A PAWM ROI including the above-mentioned 253 MS lesions was defined (Fig. 9). To segment out MS lesions, the segmentation procedure was modified to operate in two steps:

1. GM, WM, CSF, muscle, fat, globus pallidus, putamen, and PAWM voxels are classified based on their position in the multifeature space by obtaining a presegmented 3D matrix (256, 256, 32).

2. The 3D clusters composed of PAWM voxels are classified as lesion or normal tissue, taking into account their morphologic characteristics.

The second step included a) identification of "potential lesions" (PL), b) fragmentation of spatial clusters, and c) lesion classification.

1.1 Identification of "potential lesions"

The presegmented 3D matrix is scanned to find the PAWM voxels forming clusters in the physical space, which are then labeled PL. When a PAWM voxel is found, a 3D region growing technique is applied, using this voxel as a "seed," to define a spatial cluster formed by spatially contiguous PAWM voxels.

1.2 Fragmentation of spatial clusters

This step is aimed at improving classification of large lesions. In fact, the presence of large lesions increases the probability that normal tissue voxels, included in the PAWM, could be spatially connected to true lesion voxels. Thus, large PLs probably include thin connections between normal and abnormal tissues. PLs larger than 8 ml are broken up into different PL fragments using an erosion algorithm that cuts the connections thinner than 3 pixels.

1.3 Lesion classification

The aim of this task is to classify the spatial clusters based on their shape, dimension, and spatial relationship with WM. The criteria used to classify as lesion a 3D spatial cluster are based on the assumption that small MS lesions are roundish and surrounded by WM, while, as size increases, the shape becomes

more irregular, and a large interface with GM can occur. To realize this task, for each PL the following parameters are calculated:

1. PL shape factor (PLSF):

$$PLSF = \frac{n_b}{\sqrt[3]{n^2}}$$

where nb is the number of voxels surrounding the PL, n is the number of voxels of PL.

2. PL dimension factor (PLDF):

$$PLDF = \sqrt[3]{n}$$

3. Surface-volume factor (SVF):

$$SVF = \frac{PLSF^{P1}}{PLDF^{P2}}$$

where P1 and P2 are the weight factors determined in the algorithm optimization (see below).

4. Center of mass of PL and of surrounding WM (SWM) in the R1, R2, N(H) space according to the formula:

$$x_i = \frac{\sum_{j=1}^{n} x_{ij}}{n}$$

where xi is the i th coordinate of the center of mass of a tissue spatial cluster in the multifeature space, and n is the number of voxels of that cluster.

A PL is classified as lesion if the percentage of surrounding WM (SWM/nb) is greater than the surfacevolume factor. The procedure at this stage would erroneously classify as lesions some very small spatial clusters (one or two voxels) surrounded by normal WM. In fact, since in the multifeature space the

PAWM ROI is contiguous to normal WM ROI (Fig. 10), some normal WM voxels can fall into PAWM ROI due to noise; being surrounded in the physical space by WM, they would be erroneously classified as lesions.

To avoid this, a PL is classified as lesion only if the following additional condition is verified in the normalized R1, R2, N(H) space:

$$\vec{A} \cdot \vec{B} > D$$

where : $\vec{A}$ is the vector joining the centers of mass of SWM and PL, $\vec{B}$ is the unit vector oriented from the center of mass of abnormal WM to the center of mass of normal WM (obtained from the 40 studies used for optimization of the algorithm), D is the lowest distance in the parametric space necessary for detection of a lesion (ie, the minimum color contrast to detect a plaque in the QMCI images) according to two experienced neuroradiologists (A.B., M.Q.) (D 5 5.4 normalized units). The normalization of the multiparametric space was obtained by dividing spatial coordinates by NFx, NFy, NFz:

$$NFx = 1; \quad NFy = \frac{R_{1SD}}{R_{2SD}}; \quad NFz = \frac{R_{1SD}}{N(H)_{SD}}$$

where R1SD, R2SD, and N(H)SD are respectively R1, R2, and N(H) standard deviations of a manually selected pure frontal WM distribution in the same space.

If PL is not classified as lesion, it is classified as GM, WM, or CSF depending on its mean R1 and R2.

Validation

To compare the results of the fully automated segmentation program (hereinafter referred to as “unsupervised segmentation”) with manual selection of abnormal

WM (reference standard, hereinafter referred to as “supervised segmentation”), manual editing of the unsupervised segmentation results was performed using a commercial PC-based photo-editing program (Photoshop, Adobe, Mountain View, CA). The unsupervised segmentation program calculates normal and abnormal tissue volumes and provides segmented images by codifying different tissues with different colors (Fig. 11). Furthermore, it adds to each QMCI image, besides the three RGB channels containing the R1, R2, and N(H) maps, a fourth channel containing a map of the segmented MS lesions that can be displayed, as a selection, onto the QMCI images (Fig. 11). The neuroradiologist verifies the accuracy of the automated classification by comparison with the original MR images and, if that be the case, he/she can interactively modify the selection adding WM lesions not identified by the unsupervised method (false negative) or deselecting areas incorrectly classified as WM lesions by the unsupervised method (false positive). Supervised segmentation results are saved into an additional channel of the images, allowing pixel by pixel comparison of different segmentation techniques and inter-/intraoperator comparison.

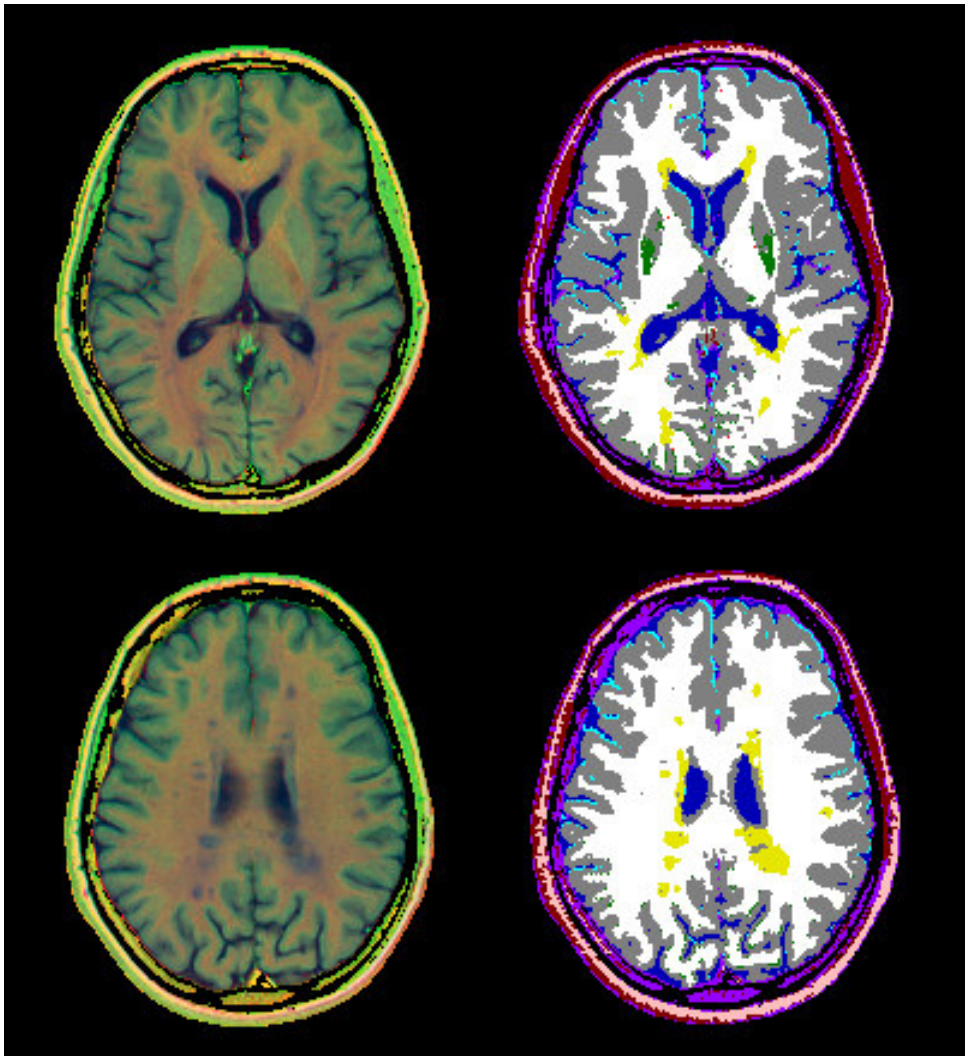

Fig. 11

Axial slices at the level of lateral ventricles in an MS patient with medium lesion load. Column on the left multifeature QMCI image are shown where MS lesions appear violet, while column on the right corresponding. unsupervised segmented image are displayed. MS lesions are displayed in yellow.

In the repeatability studies, to minimize the intraoperator variability (as required in clinical trials, when analyzing studies performed before and after therapy), simultaneous supervised segmentation of two studies was also performed. This type of analysis is hereinafter referred to as "comparative supervised segmentation."

To validate the technique, 16 MR studies in MS patients, not previously used for algorithm optimization, were analyzed with the unsupervised method and then analyzed under supervision by three experienced neuroradiologists. Furthermore, for interstudy reproducibility assessment, four patients with heterogeneous lesion load underwent two studies within the same day. No special care was taken to ensure that the same head and/or slice positioning was obtained in both studies.

1. Specificity of the method

For specificity assessment, false-positive lesion volume was defined as the amount of abnormal WM detected in ormal subjects (24 MR studies). Mean volume of the "apparently abnormal" WM detected by the unsupervised procedure in normal volunteers was 0.11 ml (range 0–0.59 ml).

2. Sensitivity of the method

Sensitivity was evaluated using the results of supervised segmentation as the gold standard: it was expressed as the percentage of WM-lesion voxels, as defined by the supervised technique, correctly classified by the unsupervised technique (true positive) in the 16 MS patients. In 16 studies in MS patients, not used for algorithm optimization, average lesion load was 31.0 ml (range 1.1–132.5). The unsupervised method correctly classified as abnormal WM 87.3% of the total lesion volume detected using the supervised technique in the 16 patients (mean sensitivity per patient 81.2%). In Fig. 5, regression of unsupervised vs. supervised technique is displayed. Slope and intercept were respectively 1.08 ± 0.03 and 1.34 ± 1.34.

3. A posteriori correction of GM and WM volumes

The segmentation technique relays mainly on calculated relaxation rates of normal brain tissues, which are fixed for each tissue and relatively independent on sequence parameters, to individuate GM, WM, CSF, and MS plaques. The only parameter tailored on each study is the R1 cutoff between GM and WM, which is calculated at a fixed percentage between the two tissue clusters (see above). However, Quarantelli et al. (Quarantelli, 2003) demonstrated the presence of a bias introduced in the segmentation of normal brain tissues by the presence of aWM (with R1 values comparable to GM), which could in theory modify the definition of the R1 threshold between GM and WM clusters.

The relationship between aWM presence and the accuracy in fractional normal tissue volumes and the resulting correction factors were reported with a posteriori correction of GM and WM volumes as assessed by linear regression analysis (Fig. 12).

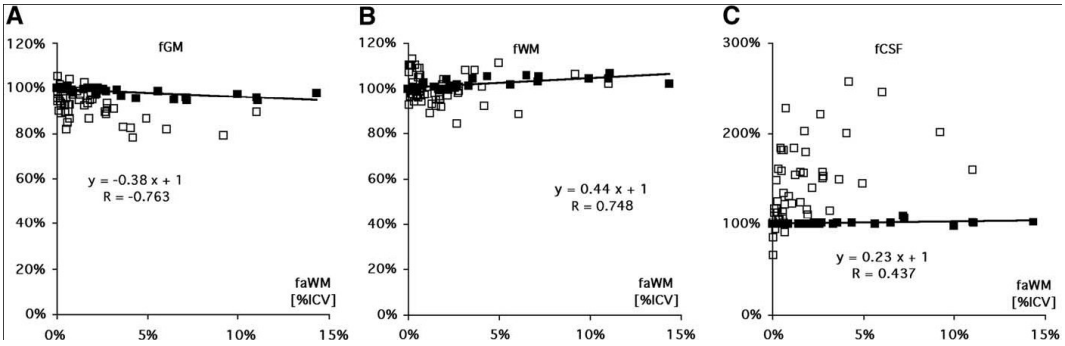

Fig. 12

Effect of the presence of aWM on the accuracy of automated measures of fGM (A), fWM (B), and fCSF (C) volumes, compared with corresponding fractional volume changes of brain normal tissues in MS patients. The fractional volumes are expressed as percentage of their original value (measured before aWM addition) for simulated MS studies (filled squares) and as percentage of the value expected for patient age in MS studies (empty squares). For simulated data, significant regression lines are reported along with corresponding equations and *R* values. A small although significant overestimation of fWM and fCSF and underestimation of fGM is detectable, largely below the observed changes in fGM and fCSF in MS patients.

BRAIN TISSUE VOLUMES IN MS: PREVIOUS RESULTS

Only a few studies have assessed volume changes in both WM and GM in mixed MS population (Liu, 1999) (De Stefano, 2001) and in purely RR (Chard, 2002; Ge, 2001; Quarantelli, 2003), but whether they are simultaneously present and sizeable is currently debated. Liu et al. reported loss in GM and WM in both RR and SP MS patients, while De Stefano at al. assessed only GM loss (he did not search for WM loss) in RR and PP separately. For the groups that studied purely RR MS patients, in one case (Ge, 2001) tissue loss appeared limited to WM, albeit a significant correlation between GM and abnormal white matter volume (aWM) was found, while a second study (Chard, 2002) found a decrease in both GM and WM fractions, although lesion load (LL) correlated only with GM loss and the third study (Quarantelli, 2003) found only a GM loss strongly correlated with LL.

Moreover, in a recent study on a group of patients with clinically isolated syndromes suggestive of MS (Dalton, 2004) GM loss (but not WM loss) was found in the subgroup of patients who developed in 3 years clinically defined MS, thus confirming the presence of GM atrophy already in the very early stages of the disease.

Although all of these studies provided consistent evidence that brain atrophy is a relevant feature of MS, the differential involvement of WM and GM in patients with different disease courses as well as the intercorrelations between WM and GM atrophy and lesion load, and the correlations between WM and GM atrophy and clinical features, have been only partially defined.

In addition none of these studies addresses the question of whether the observed tissue loss is homogeneously distributed or rather localized in specific cortical or subcortical regions.

In previous studies assessing brain tissue loss over specific pre-defined brain regions, decreases in both area and axonal density in corpus callosum (Evangelou, 2000) and in thalamic GM (Cifelli, 2002) have been reported.

Nevertheless, to date a comprehensive look at the GM regional changes has been done, to the best of our knowledge, only in one study (Sailer, 2003) using automatic surface reconstruction to measure the cortical thickness across the entire brain in a group of MS patients, including both RR and secondary progressive subtypes of the disease.

That work reported a highly significant focal atrophy bilaterally in frontal, temporal and motor areas in the MS patients, motor cortex involvement being related to physical disability.

AIM OF THE WORK

Aim of the present work was threefold:

1. to improve the multiparametric segmentation technique originally developed at our laboratory (Alfano's method) by optimizing GM/WM separation to eliminate the bias in favor of WM volumes which had been demonstrated in presence of MS lesions.
2. to quantify cerebral tissue volumes in a large population of MS patients to rule out controversies of the updated literature in the field.
3. to assess whether GM loss in MS is preferentially located in specific brain region.

For the first aim, we implemented a multigaussian fit routine to detect more accurately in each study the GM/WM R1 cutoff (i.e. the R1 value separating the GM and WM clusters). The resulting optimized segmentation routine was validated in a series of simulated MS studies.

For the second aim we sought to measure WM and GM atrophy and lesion load in a large population of patients with MS using the fully automated, operator-independent, multiparametric segmentation method previously described. The intercorrelations between WM and GM atrophy and lesion load and the correlations between clinical and MRI data were also assessed. This was accomplished by organizing a multicenter study, in which an MRI machine housed in a truck traveled to different locations to perform the same MRI protocol in all patients.

For the third aim we have used the Voxel Based Morphometry (VBM) (Ashburner and Friston, 2000), to compare on a voxel-by-voxel basis GM and WM volumes as measured by segmentation of conventional spin-echo MR images. VBM allows to compare structural features across scans of different subjects in a fully automated manner, thus overcoming problems of intra- and inter-observer bias and sensitivity, as well as the need for a-priori definition of structures of interest. We applied VBM to a selected group of RR-MS patients and to an age-matched control group to assess regional GM loss on a voxel-by-voxel basis. VBM was also used to search for an asymmetric effect of the pathology between left and right hemispheres, and to search the whole brain on a voxel-by-voxel basis for correlations between local GM volumes and disease duration, Expanded Disability Status Scale (EDSS) score and the abnormal WM (aWM) volume (hereinafter referred to as lesion load, LL).

FIRST AIM:

OPTIMIZATION OF MULTIPARAMETRIC SEGMENTATION FOR MS

To improve the segmentation method, a new technique to calculate GM/WM R1 cutoff was introduced to eliminate the previously observed slight underestimation of fGM in the presence of high LL (Quarantelli, 2003).

Calculation of GM/WM R1 cutoff with multigaussian fitting

As described in the previous chapter the Alfano's method was based on an adaptive threshold to separate in R1 WM and GM, that was recalculated for each study. Once the multiparametric maps were obtained the program calculated the histogram in R1 of all the slices in a volume and summed it to obtain an R1 distribution for each patients. As shown in Fig.12 the R1 resulting distribution for a normal subject is characterized by the presence of two peaks, the one to the left relative to GM voxel distribution and one to the right relative to WM distribution. The presence of a medium-high LL in R1 distribution due to MS plaques changes the R1 distribution increasing above normal GM peak and decreasing WM peak due to the relaxation properties of MS plaques (see Fig. 9).

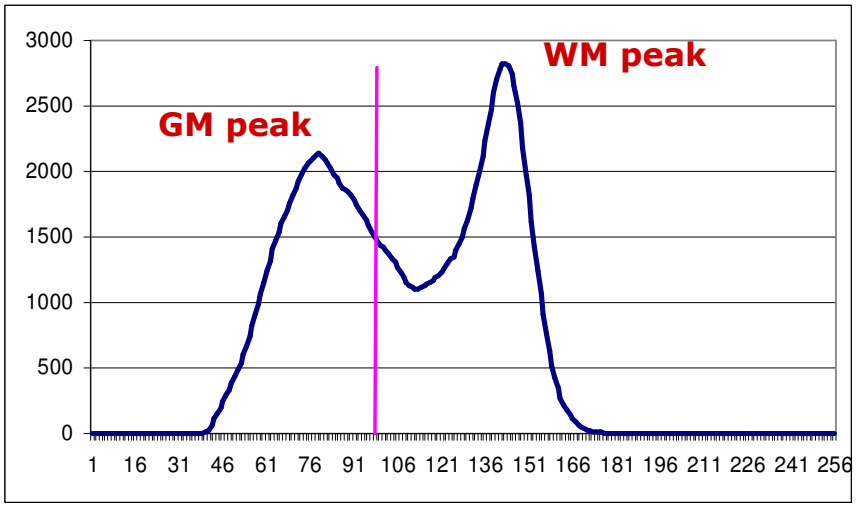

Fig. 12

R1 histogram obtained from the sum of the histograms of all slices in a volume from a normal subject. In the histogram are clearly distinguishable the GM and WM peaks. The cutoff between GM and WM, calculated as described in Alfano et al. (Alfano, 1997) is drawn in purple.

In Fig. 13 the R1 histogram of a representative MS-RR patient with a medium LL (LL=3,04% of total ICV) is shown. The cutoff between GM and WM distribution, calculated as the 43% of the distance between the two feet moves towards GM peak underestimating GM volume in favor of a overestimation of WM volume. This is due to the way of calculating the feet of the distribution as the 10% of the maximum peak that in the "normal" case is the WM peak, but in the "pathological" case could be the GM peak as shown in Fig.13.

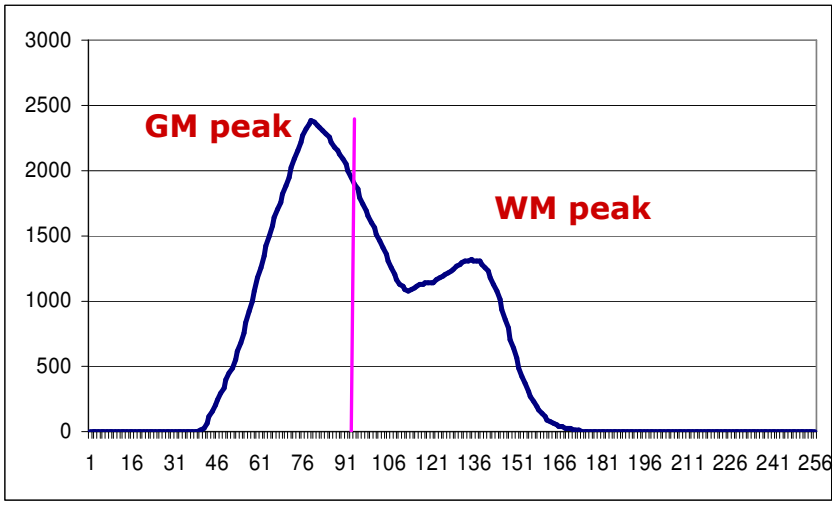

Fig. 13

R1 histogram obtained from the sum of the histograms of all slices in a volume from an MS-RR patient with a medium lesion load (LL=3,04% of total ICV). In the histogram is clearly shown the increase in GM peak due to the migration of MS plaques towards GM R1 values. The cutoff between GM and WM, calculated as described in Alfano et al. (Alfano, 1997) is drawn in purple.

To avoid correction a posteriori of the underestimation of GM volumes (Quarantelli, 2003) we introduced a new method to calculate GM/WM cutoff based on a multigaussina fitting of the R1 histogram based on the hypothesis of a Gaussian distribution of GM and WM voxel values. The procedure is now based on the following steps:

- Searching of the GM peak of the R1 distribution (blue line in Fig. 15)
- Fitting of GM voxel R1 distribution with a Gaussian function with constrains based on the rise shape of R1 histagram (purple line in Fig. 15)
- Subtraction of GM gaussian fit from R1 histogram that gives the WM pseudo-gaussian distribution (yellow line in Fig. 15)
- Calculation of the two feet of the distribution: the right feet equal to 10% of GM peak, the left feet equal to 10% for the WM peak. This new way of measuring the feet of the distribution stabilize their values even in presence of high LL.

- Calculation of the cutoff between GM and WM clusters as the 43% of the distance between the two feet (cyan line in Fig. 15)

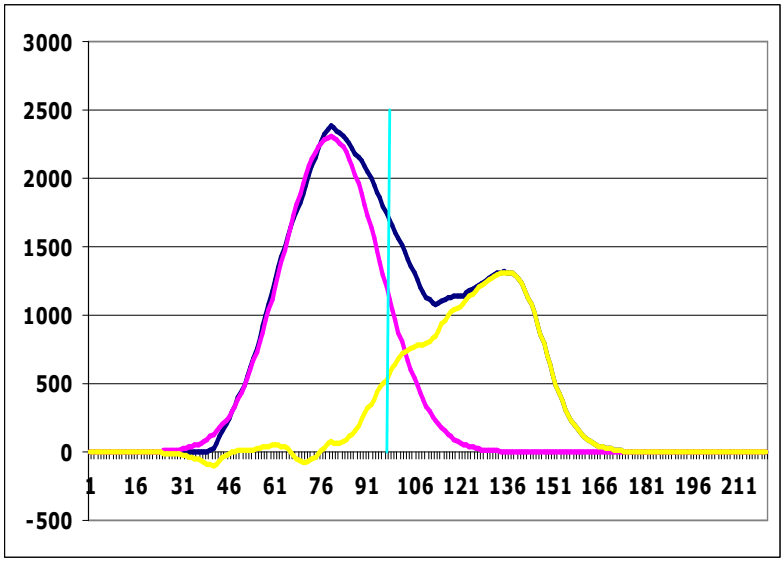

Fig. 15

Multigaussian fitting of the R1 histogram obtained from the sum of the histograms of all slices in a volume from an normal subject (blue line). Purple line shows the Gaussian fitting of the GM distribution, Yellow line indicates the pseudo-gaussian residual that fit the WM distribution, cyan line shows the threshold between GM and WM clusters.

Validation of multigaussian fitting in MS simulated studies

A validation of the accuracy of normal brain tissue volumes in the presence of aWM after the introduction of the multigaussian fitting of R1 histogram was performed, to verify the elimination of the slightly underestimation of GM volumes in the presence of medium/high LL in MS patients.

A set of simulated MS studies was thus generated by substituting in 4 NV studies variable amounts of WM with plaques selected from 4 MS studies with mid to high lesion load. The voxel clusters identified in the MS studies by the segmentation program as aWM were substituted to randomly selected areas segmented as WM in the 4 NV studies. The procedure was iteratively replicated after a 1-voxel 2D erosion of the plaques to generate 37 simulated MS studies

with progressively decreasing LL ranging from 230.2 ml to 0 (43 ± 58.7 ml; mean ± standard deviation).

The relationship between aWM presence and the accuracy in fractional normal tissue volumes were assessed by linear regression analysis (Fig. 16). The measure of GM volumes of the simulated data shows a completely recover of GM volume with a residual error (slope of the linear regression) that is less than the standard deviation of the slope of the linear regression that fits GM loss of the MS population. This demonstrated that with the multigaussian fits of the R1 histogram for the calculation of GM/WM cutoff the a posteriori correction of GM and WM volumes is not needed anymore. The software for generation of simulated MS studies was written using Interactive Data Language (IDL, Research Systems, Inc.; Boulder, CO).

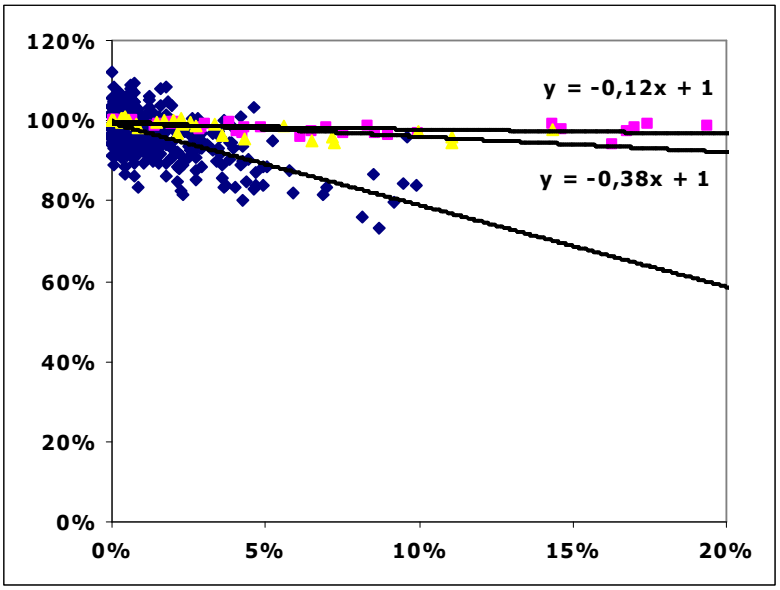

Fig. 16
Results of the simulation procedure. Blue dots represents fractional GM volumes of the MS population plotted versus fractional aWM fitted with a linear regression. Yellow dots represents the results of the simulated MS studies in the version as published by Alfano et al. (Alfano, 1997) showing the slight underestimation versus LL. Pink dots represents the GM volumes of the same simulated data with the new version of the algorithm. The slope of the linear regression is smaller that the standard deviation of the slope of the linear regression of the GM loss in MS.

SECOND AIM:

QUANTIFICATION OF GLOBAL BRAIN TISSUE VOLUMES IN A LARGE POPULATION OF MS PATIENTS

The segmentation method previously described in detail has been applied to simultaneously measure in vivo volumes of GM, normal white matter (WM), abnormal white matter (aWM), and cerebro-spinal fluid (CSF), and to assess their relationship in 50 patients with relapsing-remitting multiple sclerosis by Qurantelli et al. (Quarantelli, 2003). That work reported that brain atrophy in RR-MS mainly relates to GM loss, which in turn correlates with lesion load, global WM volume appearing unaffected by the pathology once MS plaque volume is taken into account. LL and GM loss, as well as corresponding CSF increase, do not appear to significantly affect the clinical status as assessed by EDSS, which correlates instead with disease duration. We sought to measure WM and GM atrophy and lesion load in a large population of patients with MS of mixed courses (RR, PP and SP) using the Alfano's segmentation method modified as described above and to investigate the intercorrelations between WM and GM atrophy and lesion load and the correlations between clinical and MRI data. This work was accomplished by organizing a multicenter study, in which an MRI machine housed in a truck traveled to different locations to perform the same MRI protocol in all patients.

Patient recruitment

The study design was cross-sectional. During a predefined 6-month time window, all consecutive patients with MS, on the basis of a prescheduled visit, and all consecutive 20- to 50-year-old sex-matched healthy volunteers were included. Patients with definite MS (McDonald, 2001) were recruited from the MS outpatient clinics of seven university hospitals (Second University of Naples, University "Federico II" of Naples, and Universities of Bari, Catanzaro, Messina, Catania, and Palermo) and the regional hospital of Potenza. Because these centers supply interferons (IFNs)

and other immunomodulators to patients with MS, and considering the high frequency of treatment in Italian patients with MS, it is likely that the patients of our sample are representative of the general MS population. Another selection bias may be due to the number of patients who disagreed to participate to the study. Indeed, the percentage of refusals was very low (<5%). All enrolled subjects were examined on the same day as the MRI session. Criteria for excluding patients were ongoing clinical relapse, other major medical illnesses, history of substance abuse, and corticosteroid treatment within 12 weeks of the start of the study. Criteria for excluding volunteers were neurologic disorders,

major medical illnesses, history of substance abuse, and current drug treatment. Seven hundred thirty-three subjects took part in the study: 629 patients with MS and 104 control subjects. Thirty-two patients with MS were not included in the final analysis because they did not complete the MRI exam or because of motion artifacts, so the study results are based on 597 patients with MS and 104 control subjects. The protocol was approved by local ethics committees. All participants gave written informed consent.

MRI studies

The same MRI protocol was performed in all subjects using the same MRI scanner (1.0 T Genesys Signa; GE Medical Systems, Milwaukee, WI). For each study, two interleaved sets of 15 slices (4 mm thick) covering the entire brain were acquired, using for each set two conventional spin echo sequences (repetition time/echo time [TR/TE] 600/15 milliseconds, two averages; TR/TE 2300/15 – 90 millisecond dual-echo sequence, one average; both with 90° flip angle and 256 x 192 matrix). All the studies were segmented using a the fully automated Alfano's method, based on relaxometric characterization of brain tissues. The program gives complete sets of multifeature images (R1 [=1/T1], R2 [= 1/T2], proton density [N(H)-based]) and segmented images and calculates the volumes of the following intracranial tissues: CSF, GM, normal appearing WM, abnormal WM (aWM), and global WM (gWM; calculated as the sum of normal appearing WM and aWM). To normalize for head size variability, the volumes of intracranial tissues were expressed as fractions (f) of the intracranial volume, which were calculated for each subject as the sum of all intracranial tissues. faWM is a measure of lesion load as determined by the R1, R2, and N(H) information and morphologic characteristics, the reduction of fWM indicates WM atrophy, and the reduction of fGM indicates GM atrophy.

For each study, a couple of interactive interslice movies of both multispectral and segmented images were produced, and two neuroimaging experts reviewed them (for a maximum of 2 minutes) to detect motion artifacts and segmentation errors due to the imperfect separation of nasal mucosa and vitreous humor from brain

issue. In 111 studies (15.8%) in which nasal mucosa or vitreous humor was erroneously classified as GM or CSF, manual cuts of thin connections between intra- and extracerebral tissues in the multispectral image set were performed, allowing the program to outcome correct segmentation and volumetry.

Results of the segmentation of a large population of MS patients

The study population of patients with MS consisted of 383 women and 214 men (women/men ratio = 1.8) ages 16 to 68 years (mean ± SD 38.1 ± 10.3 years). Their age at disease onset was 10 to 61 years (28.4 ± 9.1 years), and their EDSS scores19 were 0 to 8.5 points (2.99 ± 1.7 points). Disease duration was 9.73 ± 7.26 years, and number of relapses in the previous 2 years was 1.04 ± 1.3. The clinical course was RR in 427 (71.5%), SP in 140 (23.5%), and PP in 30 (5.0%). EDSS score was = 3.5 in 452 patients (88.3% RR, 7.5% SP, 4.2% PP), between 4 and 6 in 110 patients (22.7% RR, 60.9% SP, 16.4% PP), and = 6.5 in 35 patients (57.1% SP, 42.9% PP).

Measurements of segmented MRI volumes in the patients with MS and controls are presented in Fig. 17. fGM (blue dots), fWM (yellow dots) and CSF (pink dots) of MS patients are plotted versus faWM with the corresponding linear regression fitting. fGM and fCSF values are age-corrected based on fGM and fCSF volume changes with age derived from NV populations. fWM do not show any change with age and do not need to be corrected. As depicted in Fig. 17 both fGM, fWM loss in MS patients are strongly correlated with faWM ($p < 0.001$) with a corresponding increase in fCSF.

In patients with MS, the mean value of faWM was 1.4% 95% CI 1.3 to 1.5), which corresponds to a lesion load of about 17 cm^3 in an average brain of 1200 cm^3. fWM was ($p < 0.001$) reduced in patients with MS by 1.3% (95% CI 0.5 to 2.1), which corresponds to a volume loss of about 15.6 cm^3 in an average brain of 1200 cm^3. fGM was reduced ($p < 0.001$) in patients with MS by 2.1% (95% CI 1.4 to 2.8), which corresponds to a volume loss of about 25 cm^3 in an average brain of 1200 cm^3.

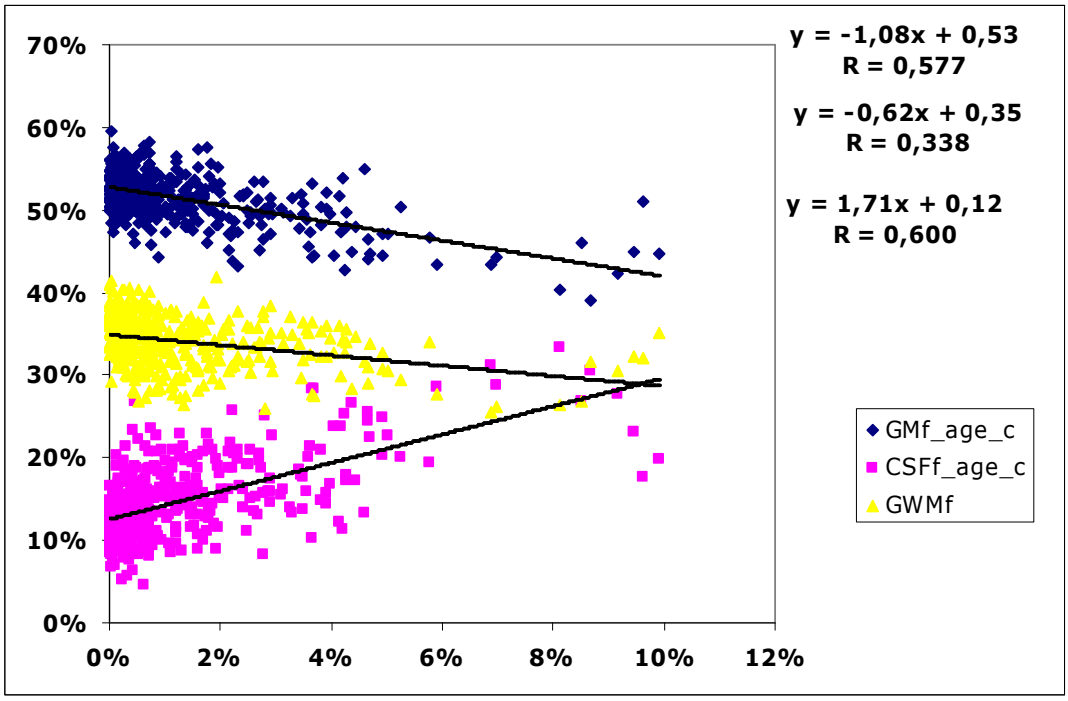

Fig. 17

Scatterplot of fGM (blue dots), fWM (yellow triangles), and fCSF fraction (pink boxes), vs faWM. fGM and fCSF values are adjusted to patients mean age (38.3 years). Where significant, regression lines are reported along with the corresponding equations and R values. Increasing loss of GM and WM (which includes also the WM lesion volume) with corresponding increase in CSF is apparent with increasing faWM.

Table 1 shows the comparisons of segmented MRI volumes in patients with MS with different disease courses. Between-group comparisons showed significant

differences of MRI parameters only in RR patients with respect to SP patients. Both fWM and fGM were significantly lower in the SP group than in the RR group. The magnitude of the fWM reduction was similar to that of fGM, being 1.4% (95% CI 0.8 to 2.0) for both. Furthermore, faWM was significantly higher in the SP group than in the RR group (0.7%; 95% CI 0.3 to 1.1).

	Mean (95% CI					
	RR, n=427	SP, n=140	PP, n=30	RR vs SP	RR vs PP	SP vs PP
faWM	1.2 (1.0-1.4)	1.9 (1.6-2.2)	1.8 (1.2-2.5)	<0.001	NS	NS
fWM	34.2 (33.9-34.5)	32.8 (32.3-33.4)	33.1 (31.9-34.2)	<0.001	NS	NS
fGM	51.4 (51.1-51.7)	50.0 (49.4-50.5)	50.7 (49.2-51.5)	<0.001	NS	NS

* Adjusted for age, sex, and education

Table 1

Comparisons of adjusted* MRI volumes (as % of whole brain volume) for different MS courses
RR= relapsing-remitting, SP= secondary progressive, PP= primary progressive, AWM-f=abnormal WM fraction, gWM-f = global WM fraction, GM-f= GM fraction

From the multivariate correlations of MRI fractions with clinical features, three significant predictors of lesion load were obtained: EDSS, age at disease onset, and drug treatment (IFNβ vs never treated). The strongest predictor was disability: a 1-point increase in the EDSS score corresponded to about a 0.24% increase of faWM 2.9 cm3 for an average brain of 1200 cm3). Furthermore, a 0.15% increase of faWM was found for each 5 years earlier that the MS had its onset.

IFNβ-treated patients had a higher lesion load (adjusted mean of 1.6%; 95% CI 1.4 to 1.7) than did patients who had never been treated (1.2%; 95% CI 1.0 to 1.5, $p < 0.008$).

With regard to WM atrophy, the strongest predictor was age at onset followed by disability: a 0.45% decrease of fWM was found for each 5 years earlier of MS onset. Furthermore, a 1-point increase in the EDSS score corresponded to about a 0.41% decrease of fWM(about 5 cm3 for an average brain of 1200 cm3).

THIRD AIM:

REGIONAL ANALYSYS OF GRAY MATTER AND WHITE MATTER LOSS IN RELAPSING-REMITTING MULTIPLE SCLEROSIS

In the final part of the work we addressed the question of if and where GM and WM loss in MS patients is localized by means of optimized Voxel-Based Morphometry method applied to MRI studies of a population of patients with clinically defined Relapsing-Remitting MS and a population of age-matched normal subjects, segmented into normal and abnormal brain tissues using the modified version of Alfano's method described above. Segmented GM and WM volumes where subsequently compared on a voxel-by-voxel basis to highlight regions of relative GM and WM loss ($p<0.05$, corrected for multiple comparisons at AnCova).

Additionally, localized differences in brain asymmetry between the MS and the control groups were assessed by comparing on a voxel-by-voxel basis maps of GM differences between the two hemispheres ($p<0.05$ corrected for multiple comparisons).

Subjects

Eighty-three patients with clinically defined multiple sclerosis according to Poser criteria (Poser, 1983) with a RR course (Lublin and Reingold, 1996) (54 female) and thirty-four normal volunteer (NV, 15 female) were recruited in the study. The mean age of the patient group was 38.6 ± 7.5 years (age range 17 – 58), with a

mean disease duration of 11 ± 6.8 years (range 0 – 34) and a median EDSS (Kurtzke, 1983) score of 2.6 (range 1 – 6). All patients had been previously treated only by brief courses of steroids during clinical exacerbations. Mean age of the NV group was 43.2 ± 13.2 (range 22 – 69). Exclusion criteria for NV were evidence of cardiovascular, metabolic, neurological, and psychiatric impairment, as well as abnormal MRI examination. All MS patients and NV were right-handed.

Both NV and MS patients agreed to participate in the study by signing a written informed consent, and the ethical committees of participating Institutions previously approved the protocol.

MRI studies

MRI protocol included two interleaved sets of 16 slices each covering the whole brain obtained at 1.5 T (Intera, Philips Medical Systems, The Netherland), sampling the brain at a total of 32 contiguous levels. Each of the two sets included conventional spin-echo sequences providing T1w (520/15 msec TR/TE) and PD/T2w (1800/15-90 msec TR/TE) 4mm-thick axial images (24cm FOV, 256x256 acquisition matrix). Images from all studies were segmented using Alfano's method in the modified version previously described.

Optimized VBM

Voxel Based Morphometry (Ashburner and Friston, 2000) was used in an optimized version (Good, 2001b) to process and analyze segmented GM and WM maps using Statistical Parametric Mapping software (SPM2, Wellcome

Department of Cognitive Neurology, London, UK, www.fil.ion.ucl.ac.uk/spm) (Friston, 1995) running under MATLAB version 6 (the Mathworks, Inc., MA, USA).

To minimize potential normalization problems related to differences of registration to the standard space between normal and pathological brains (Karas, 2003), we created a site- and study-specific template. This was done by firstly normalizing the segmented GM volumes of each subjects (both NV and MS) to a standard space with a 12-parameter affine model without any nonlinear component (Ashburner, 1997). The GM prior provided with SPM2 was used as standard space model. The resulting roughly normalized GM images of all the subjects were averaged, and the resulting volume was smoothed with a Gaussian filter of 8 mm full-width at half-maximum (FWHM) (Fig. 18). Nonlinear components were not used for template creation in order to preserve group affine geometry (Woods, 1998).

The use of a site- and group-specific template, created including both normal and pathological volumes, reduces systematic registration bias to any of the two groups.

GM maps of each subject were then normalized to the GM specific template by performing affine registration and 16 nonlinear iterations using 6 x 8 x 6 basis functions to account for global nonlinear shape differences (Ashburner and Friston, 1999). Normalized images were resampled by trilinear interpolation to 1 x 1 x1 mm voxel size. In addition WM maps were normalized by means of the GM normalization matrices and resampled by trilinear interpolation to 1 x 1 x 1

mm voxel size. The use of GM normalization matrices for WM analysis, rather than building a WM specific template, was choose to minimize normalization errors since GM normalization matrices gave more reperee on head shape.

For each patient study, we also applied the GM-derived normalization matrix to corresponding aWM volume and averaged the resulting normalized aWM volumes to visually assess plaque distribution in our patient population (Fig.18), and to derive left and right hemisphere lesion load for subsequent symmetry analysis (see below).

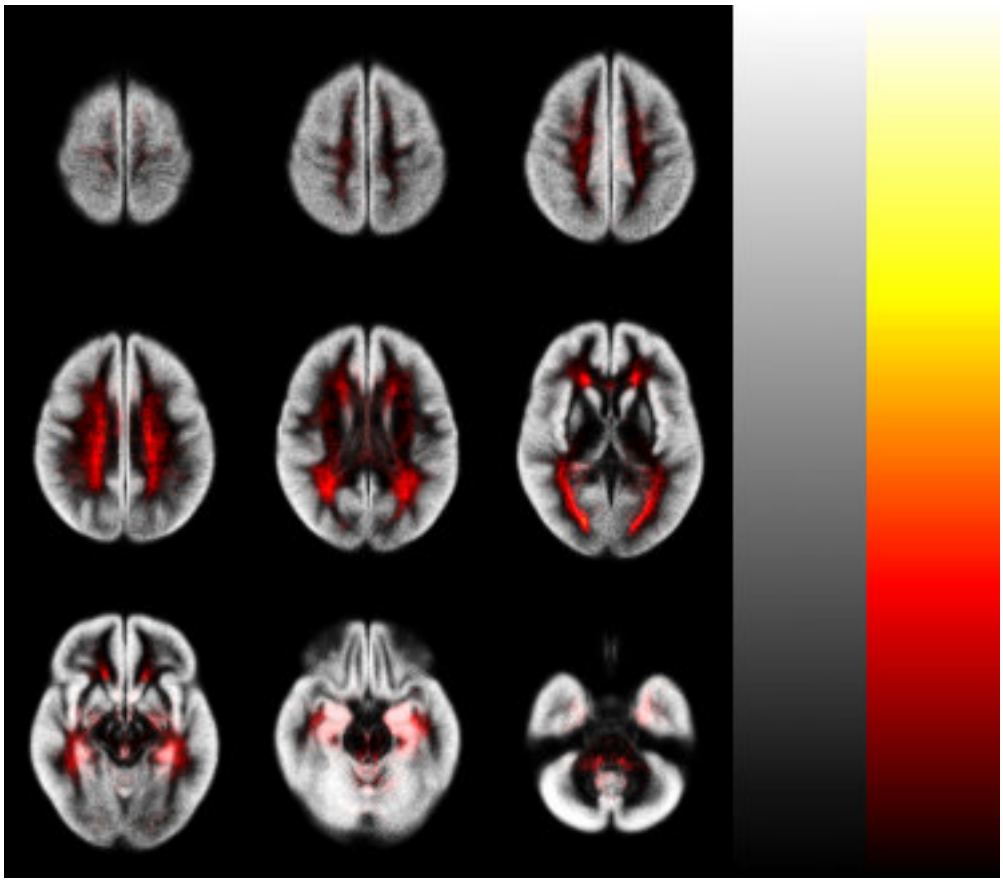

Fig. 18

Mean of the normalized distribution of aWM in the patient population (in colour scale) superimposed to the unsmoothed GM template (in greyscale). Images are scaled to their own maximum. Plaques are almost symmetrically distributed and concentrated more toward the posterior part of the brain leaving the centrum semiovalia almost unaffected.

Since nonlinear normalization implies that certain regions of the brain expand or contract to match the template, it was important to correct for the effect of these deformation onto regional volumes, as our goal was to assess regional change in GM and WM volumes. This was done by "modulating" the voxel values of the normalized maps to preserve the total tissue volume in the images, meaning that areas that were expanded during normalization were correspondingly reduced in values to preserve the information on their original size while the values of the voxels from shrunken areas were correspondingly increased.

Modulation was performed by multiplying GM and WM voxels by the Jacobians derived from spatial normalization to preserve the amount of the specific tissue in each voxel (Ashburner and Friston, 2000).

Finally, modulated images were smoothed with a 12-mm FWHM isotropic Gaussian filter to reduce confounding by individual variations in gyral anatomy and to render the data more normally distributed as per the Gaussian random field model underlying the statistical process used for adjusting p values (Ashburner, 1997).

It should be noted here that the optimized VBM method, as described in literature, implies a preliminary iterative normalization/segmentation procedure to improve the accuracy of segmentation. This was however not needed in our case, as the segmentation technique that we used is not based on prior probability distributions in a normalized space, and as such does not need a preliminary normalization to create site-specific GM, WM and CSF priors.

Also the erosion/dilation procedure described by Karas at al. (Karas, 2003), introduced in optimized VBM to eliminate the misclassification of voxels lying at

the interface of ventricular CSF and periventricular white matter, was not needed in our case as this segmentation error was not appreciable in our GM maps (Fig.18).

Statistical analysis

The effect of the disease onto GM volumes was preliminarily tested by stepwise multiple regression analysis using SPSS (SPSS Inc., Chicago, Il, USA). Total intracranial volume (ICV, derived from the sum of GM, normal WM, abnormal WM, and CSF), age and sex were entered first in the model to account for the possible effects of these variables.

Subject group (NV versus MS patient) was then entered to explore the effect of the disease.

Normalized modulated GM and WM maps were statistically analyzed using the general linear model based on the random Gaussian field theory (Friston, 1995).

The design matrix was constructed to test for regional differences in GM and WM respectively between RR-MS group and normal subjects. To take into account their effect on brain tissue volumes, age and sex were entered as nuisance regressors (confounding covariates) in an analysis of covariance (AnCova), while ICV was entered in the model to normalize for head size (Friston, 1995). Prior to regression analysis scans were thresholded at 40% of global intensity to reduce the influence of any remaining non-brain tissue. This analysis allows to test for morphological differences between the two groups across the whole brain on a voxel-by-voxel basis; a threshold of $p<0.05$ was used, corrected for multiple

comparisons at the voxel level. Both positive (NV > MS) and negative (NV < MS) contrasts were calculated.

The effect of LL and clinical parameters (EDSS and DD) onto GM volumes was preliminarily assessed by performing VBM on subgroups of MS patients defined based on clinical parameters.

To test for effect of LL, MS patients were divided in two groups: 59 patients with LL < 2% of total ICV (mean = 0.94 %, range 0.07 – 1.97) and 24 patients with LL > 2% of ICV (mean = 3.53%, range 2.12 – 7.08). The cutoff of 2% was the mean value of the total population.

To test for the effect of DD, MS patients were divided into three groups of almost equal size: 30 patients with DD < 8 years (mean = 4.4 yy, range 0 – 7.8), 26 patients with 8 < DD < 13 years (mean = 10.68 yy, range 8.1 – 12.7), 27 patients with DD > 13 years (mean = 18.8 yy, range 13 – 33.3).

To test for the effect of EDSS patients were divided in two groups: 53 patients with EDSS $\leq$ 2.5 (mean = 2.01, range 1 – 2.5). The cutoff was selected to separate mild to moderate severity.

Each of the above group was statistically compared on a voxel basis to the NV group.

Additionally, voxel-wise linear regression analysis between probability of grey-matter and EDSS, disease duration, and LL, was performed with age and sex as nuisance covariates, to identify clusters of voxels whose grey-matter density relates to these parameters; a threshold of $p<0.05$ was used, corrected for multiple comparisons at the voxel level.

Analysis of brain asymmetry

Localized GM loss, if preferentially located on one side of the brain, would alter the physiologic asymmetry pattern of the normal brain.

To explore this possibility, we checked for differences in brain asymmetry between the MS and the control groups by using an analysis technique similarly to what previously done by Luders et al. (Luders, 2004).

First, a symmetric site- and study-specific template was created by flipping left-right the GM normalized images from all subjects used to create the GM template for VBM. The resulting normalized flipped GM images of all the subjects were averaged together with the unflipped ones and smoothed with a Gaussian filter of 8 mm full-width at half-maximum (FWHM) to create a symmetric GM template (Good, 2001a; Luders, 2004). The GM original images of all the subjects were normalized to the symmetric GM specific template by performing affine registration and 16 nonlinear iterations using 6 x 8 x 6 basis functions as for optimized VBM. Normalized images were modulated and resampled by trilinear interpolation to 1 x 1 x1 mm voxel size. To verify for the presence of statistically significant differences in asymmetry between MS and NV groups we generated for each subject a new set of images, the Asymmetry Index maps, as described in detail by Luders et al. (Luders, 2004), that represent the GM differences between the two hemispheres. The Asymmetry Index maps of the two groups were compared using a one-way analysis of covariance (AnCova) with age and sex entered as nuisance variables.

This analysis was meant to integrate the VBM analysis by exploring, if localized GM loss was detected, if it was significantly lateralized, a condition which would

induce a significant difference between the asymmetries of MS group respect to NV. The statistical map was thresholded at a level of $p<0.05$, corrected for multiple comparisons.

Additionally, hemispheric lesion loads were tested to detect any asymmetry in aWM distribution between the two hemispheres using paired t-test.

Results

The preliminary analysis of global GM volumes confirmed previous findings (Chard, 2002; Quarantelli, 2003) of GM loss in MS patients as compared to NV (607.7 ± 66.1 ml vs. 660.1 ± 49.7 ml, respectively corresponding to 45.7% and 47.0% of ICV), the difference being significant at multiple regression analysis ($p<0.001$). WM loss also in our population of MS patients results reduced as compared to NV (499.8 ± 64.9 ml vs. 562.2 ± 66,8 ml, respectively corresponding to 37,4% and 39.88% of ICV)

MS patients showed a moderate LL, aWM volume being 22.8±18.8 ml (range 1.8 84.9).

In figure 18 the site- and study-specific unsmoothed GM template is displayed in greyscale. Superimposed in colour scale is the average distribution of aWM in the 83 MS studies, showing a mostly supratentorial, periventricular symmetric distribution. Clusters of significant GM loss in RR-MS as compared to NV after correcting for age, sex and ICV are illustrated in figures 19 and 20. Significance level is set at $p < 0.05$, corrected for multiple comparisons at voxel level.

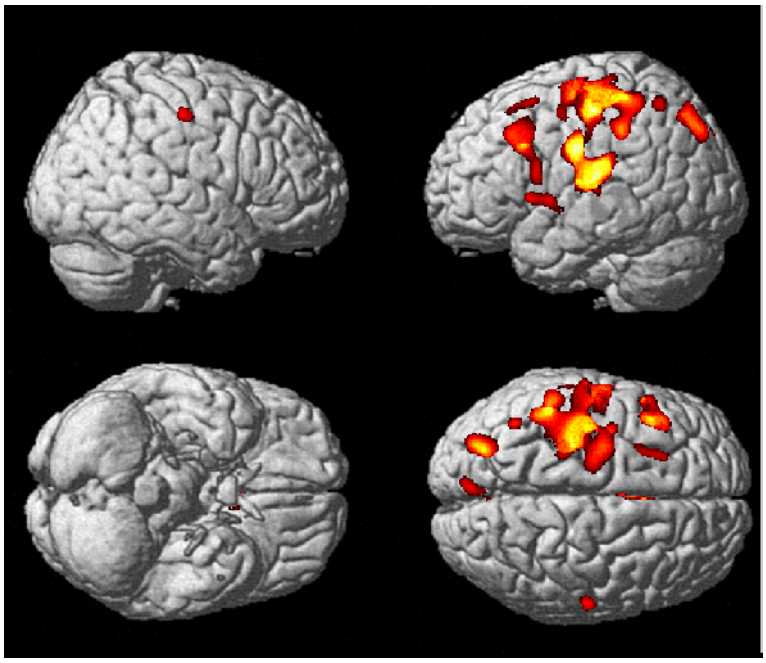

Fig. 19

Regions of significantly reduced cortical GM volume in RR patients ($p<0.05$ corrected for multiple comparisons at voxel level, i.e. T-score > 4.79) as compared to normal subjects. Significant clusters are overlaid in colour scale onto the surface of a single subject normalized brain.

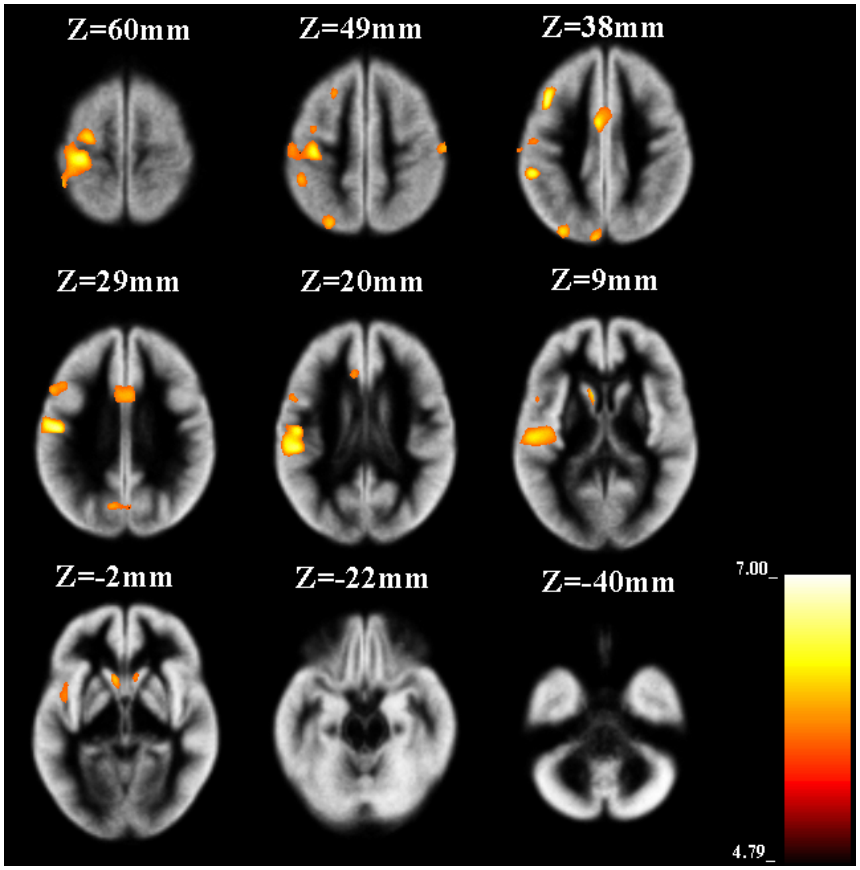

Fig. 20

Axial sections (patient's left side is on the observer's left side) from selected levels of the unsmoothed GM template (in greyscale). The regions of significant GM loss in MS patients are overlaid (in yellow).

For each cluster, the size, involved Brodmann Areas (BA) and the Talairach coordinates of the peak are reported in Table 2.

Clusters of significant GM loss in RR-MS patients were located predominantly in the left dorso-lateral frontal lobe, including motor area (BAs 4 and 6) extending into the transverse temporal gyrus (BA 41), as well as Brodmann areas 8, 9 and 44.

Other clusters of significant GM loss were located bilaterally in the anterior cingulate gyrus (BA 24) and caudate heads, as well as in the left precuneus (BA19) extending into the left parietal lobule (BA 40) and cuneus (BA 7), left insula (BA 13) extending into superior temporal gyrus (BA 22) and right postcentral gyrus (BA 3).

The search for inverse contrasts (increase tissue volumes in MS patients) did not show any significant region.

					Coordinates (mm)		
Region	**Side**	**BA**	***N. voxel***	**T**	***x***	***y***	***Z***
Precentral Gyrus	**L**	**4/6**	**20085**	**6.96**	**-32**	**-24**	**52**
Transverse Temporal Gyrus	L	41					
Middle Frontal Gyrus	**L**	**9/8**	**3080**	**6.41**	**-42**	**22**	**33**
Precentral Gyrus	L	44					
Inferior Frontal Gyrus	L	9					
Superior Frontal Gyrus	L	6					
Cingulate Gyrus	**bilateral**	**24**	**3251**	**5.97**	**-4**	**3**	**35**
Caudate Head	**L**	**n/a**	**910**	**5.97**	**-7**	**14**	**1**
Precuneus	**L**	**19/31**	**1703**	**5.85**	**-30**	**-76**	**79**
Parietal Lobule	L	40/7					
Cuneus	L	7					
Postcentral Gyrus	**R**	**3**	**323**	**5.56**	**59**	**-14**	**45**
Insula	**L**	**13**	**680**	**5.31**	**-44**	**13**	**0**
Superior Temporal Gyrus	L	22					
Caudate Head	**R**	**n/a**	**217**	**5.28**	**9**	**15**	**-2**

Table 2

Clusters of significant GM loss in RR-MS patients, relative to controls. For each cluster are reported the extension and the corresponding Brodmann Areas (BA) in which local maxima are located, along with the coordinates in the Talairach space (Talairach and Tournoux, 1988) and the T level of the most significant voxel.

n/a: not applicable

The results of the GM asymmetry analysis are displayed in Figure 21. A cluster of reduced GM is present on the left in MS, extending from pre-rolandic cortex to the superior temporal area, co-localized with major GM loss regions, , confirming

a preferential left-sided GM loss at this level. aWM did not show a significantly asymmetric distribution across the two hemispheres, left hemisphere containing 49.0% ± 12,2% of LL, the difference between the two hemispheres not being significant at paired T-test (P=0.53).

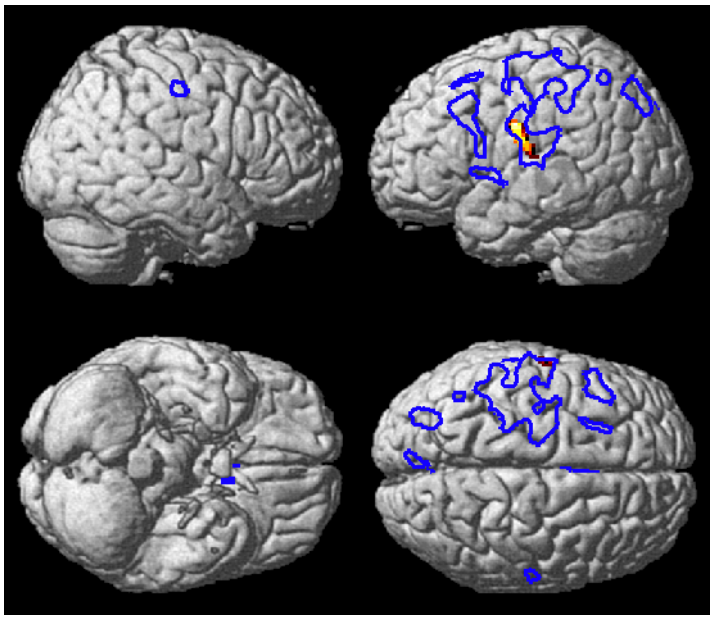

Fig. 21

Region of significant differences in GM asymmetry in RR patients ($p<0.05$ corrected for multiple comparisons, i.e. T-score > 4.93) as compared to normal subjects. The significant cluster of reduced GM in RR patients is overlaid in colour onto the surface of a single subject normalized brain. Contours of the regions of GM loss resulting from VBM analysis are overlaid in blue.

No significant correlation emerged between regional GM volume EDSS and disease duration.

Results of the voxle-wise linear regression analysis between GM loss and LL is shown in Fig. 23 ($p<0.05$ was used, corrected for multiple comparisons at the voxel level).

Regions of significantly reduced cortical GM volume in RR patients that linearly correlated with LL are preferentially located at the level of right and left caudate heads, left hippocampus, right and left primary motor areas and left and right frontal lobe.

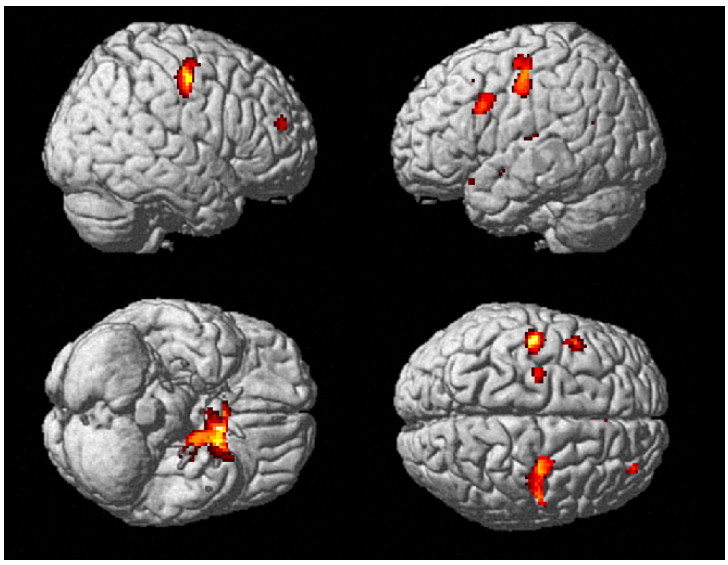

Fig. 23

Regions of significantly reduced cortical GM volume in RR patients that linearly correlated with LL ($p<0.05$ corrected for multiple comparisons at voxel level, i.e. T-score > 4.63). Significant clusters are overlaid in colour scale onto the surface of a single subject normalized brain.

Clusters of significant GM loss in the subgroups of MS patients on the basis of their LL, DD and EDSS as compared to NV after correcting for age, sex and ICV are illustrated respectively in figures 24, 25 and 26. Significance level is set at $p < 0.05$, corrected for multiple comparisons at voxel level.

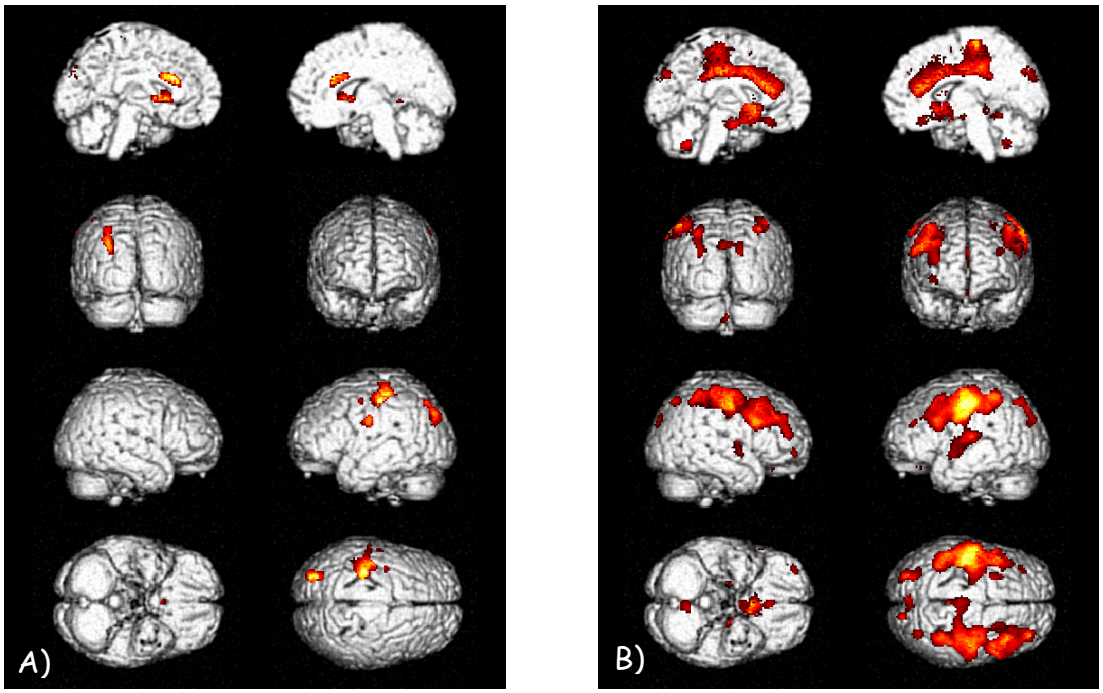

Fig. 24

Regions of significantly reduced cortical GM volume in two subgroups of RR patients: A) 59 patients with LL < 2%, B) 34 patients with LL > 2% ($p<0.05$ corrected for multiple comparisons at voxel level, i.e. T-score > 4.7). Significant clusters are overlaid in colour scale onto the surface of a single subject normalized brain.

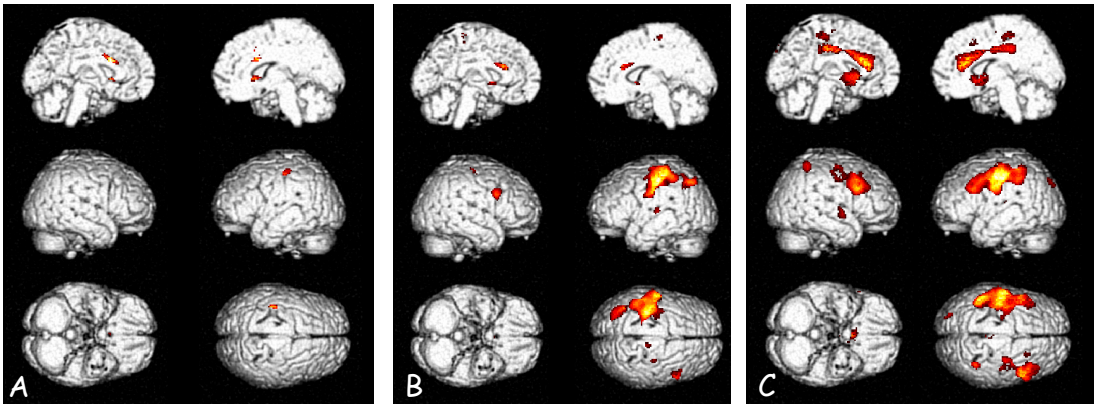

Fig. 25

Regions of significantly reduced cortical GM volume in three subgroups of RR patients: A) 30 patients with DD < 8 years, B) 26 patients with 8 < DD < 13 years, C) 27 patients with DD > 13 years ($p<0.05$ corrected for multiple comparisons at voxel level, i.e. T-score > 4.7). Significant clusters are overlaid in colour scale onto the surface of a single subject normalized brain.

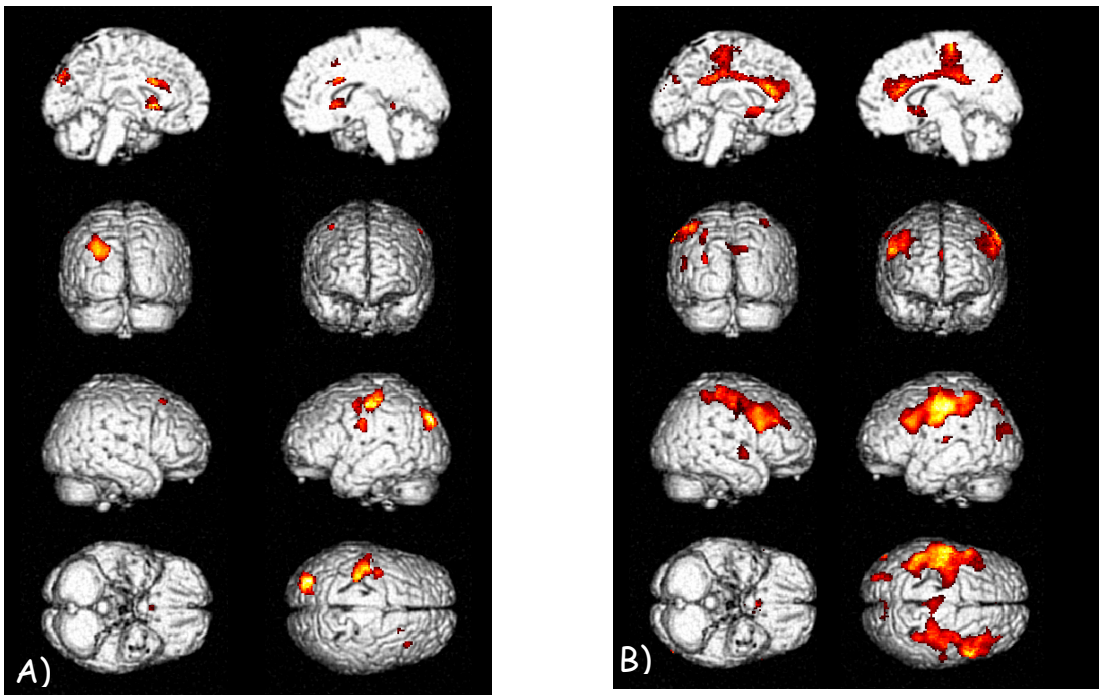

Fig. 26

Regions of significantly reduced cortical GM volume in two subgroups of RR patients: A) 53 patients with EDSS < 2.5, B) 30 patients with EDSS > 2.5 ($p<0.05$ corrected for multiple comparisons at voxel level, i.e. T-score > 4.7). Significant clusters are overlaid in colour scale onto the surface of a single subject normalized brain.

For all of the parameters tested regions of significantly reduced GM as LL, EDSS and DD increase showed a good co-localization with GM reduced regions of the entire population.

Clusters of significant WM loss in RR-MS as compared to NV after correcting for age, sex and ICV are illustrated in figure 22. Significance level is set at $p < 0.05$, corrected for multiple comparisons at voxel level. WM loss is almost symmetrically distributed and preferentially located at the level of supratentorial periventricular regions.

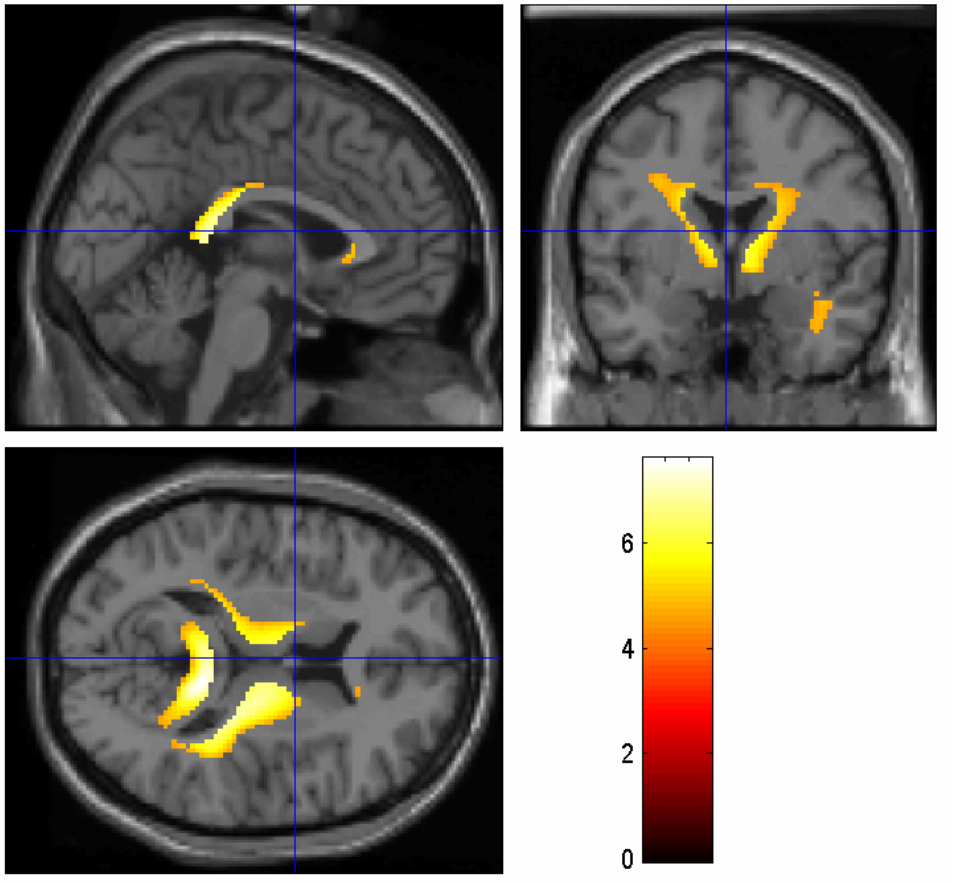

Fig. 22
Regions of significantly reduced WM volume in RR patients ($p<0.05$ corrected for multiple comparisons at voxel level, i.e. T-score > 5.12) as compared to normal subjects. Significant clusters are overlaid in colour scale onto the MR volume studies of a single subject normalized brain.

DISCUSSION

In this work, a fully automated segmentation technique was used in an optimized version in a large MS population to assess both WM and GM atrophy and lesion load as well as to investigate the intercorrelations between MRI measurements of atrophy and lesion load and the correlations between clinical and MRI data.

We have also applied an optimized VBM method to a selected group of RR-MS patients to investigate regional GM and WM loss in this specific disease subtypes.

Our results demonstrated a preferential left-sided fronto-temporal GM loss, with other areas located in the left precuneus and bilaterally in anterior cingulate gyrus and caudate nuclei.

These results integrate previous findings demonstrating global GM volume reduction selectively in RR MS (Chard, 2002; Ge, 2001; Quarantelli, 2003).

However, before discussing findings both on global values and in the localization/lateralization of GM loss, as well as possible implications on our understanding of the underlying mechanisms, some methodological issues, pertaining to both segmentation and VBM, should be examined.

Methodological Issues: segmentation

We used a fully automated procedure, based on segmented 2D conventional SE MR images, which is suitable for the analysis of data from large clinical trial, which typically do not include high-resolution 3D volumes. With this respect it is of note that the accuracy of the multiparametric segmentation method when analysing 4mm thick slices has been validated in previous work (Alfano, 1998),

while the use of 4mm thick slices is unlikely to affect VBM, which includes a three times larger smoothing (12mm FWHM).

The multiparametric segmentation method was modified to increase the robustness of GM/WM separation in presence of aWM, demonstrating over simulated MS studies a high degree of accuracy in determining the GM volume.

Although a region-specific lesion-associated segmentation bias may still be present in our data, it should be considered that such an error would result in a regional GM loss strongly correlated with LL, a finding which is not present in our results, apart from the caudate nuclei, which however have been demonstrated to be affected also using manual parcellation methods (Bermel, 2003).

Consequently, these results are not explained by a region-specific lesion-associated segmentation bias.

Also, the presence of juxtacortical plaques could in theory have biased our results by inducing underestimation of the adjacent grey matter. However the assessment in the same standard space of the regions of GM loss and of the mean aWM distribution suggests that this is not the case at least for the frontal cortex, which is far from the bulk of the LL, located in the periventricular region.

Finally, the presence of intracortical lesions may additionally have induced individual variability in the GM by altering the segmentation of adjacent GM, introducing an inter-individual local variability that may partly obstruct the detection of local GM differences. It should be however considered that signal intensity changes in intracortical plaques are subtle at MRI (Kidd, 1999), reducing their possible effects onto the segmentation procedure, especially in a population with a relatively low lesion load as in this case.

Methodological Issues: VBM

Several factors may affect the capacity of VBM to detect regional GM loss, including physiological inter-individual variability in the NV cohort (which may preclude the detection of subtle changes in MS patients), the heterogeneity intrinsic to the pathology (which may be enhanced when different disease durations are included), and noise of the measurement (derived from noise of the MR images and from segmentation and normalization errors). Additionally, it should be considered that all these factors may in principle have a different effect in different areas of the brain which in turn may render VBM differently sensitive to atrophy in different areas of the brain.

However the relative sparing of the occipital lobe and of the infratentorial regions, emerging from our findings, is compatible with previous studies showing a significant preservation of infratentorial structures in MS patients with mixed disease courses (Sailer, 2003), as well as in RR-MS as compared to secondary progressive MS patients (Edwards, 1999).

Global tissue volumes

Overall, compared with controls, patients with MS had more atrophy of both WM (−1.3%) and GM (−2.1%), and the burden of MS on brain volume, with respect to an average brain of 1200 cm3, can be summarized by the appearance of 17 cm3 of faWM and by the lack of about 16 cm3 of fWM and 25 cm3 and of fGM. In more detail, patients with MS lost 17 cm3 of WM because of MRI-identifiable lesions (faWM) and 16 cm3 because of volumetric measurable atrophy (fWM). Our

results are in agreement with previously published data (Chard, 2002) which described, in 26 patients with MS, a significant reduction of both WM (approximately −4.9%) and GM fractions (approximately −2.8%). The slight differences in the amount of WM and GM atrophy may be due to a large difference in the number of patients studied, although a difference in the segmentation methods cannot be ruled out. In a small group of RR patients, the loss of parenchymal volume in RR MS was predominantly confined to WM (Ge, 2001). With use of the same segmentation method in 50 patients with RR MS, a significant reduction of fGM was found, whereas fWM was not significantly different between patients and control subjects (Quarantelli, 2003). The lack of significant WM atrophy may be due to the small sample of RR patients studied.

A T1-weighted segmentation method was used to separate segmented GM into neocortical and non-neocortical in 90 RR and PP patients, and a significant reduction of neocortical GM was found in both groups of patients (De Stefano, 2003).

Compared with previous studies, we produced more comprehensive evidence that there is significant atrophy of both GM and WM in patients with MS, thus confirming the pathologic evidence (Cifelli, 2002; Kidd, 1999; Peterson, 2001; Trapp, 1998) of GM involvement in MS.

Among the studies based on automated MR segmentation methods, only one (De Stefano, 2003) assessed differences between patients with different disease courses and found no significant differences in neocortical GM between RR and PP patients. In our work, we showed that SP patients, with respect to RR ones, have significantly more atrophy of both GM and WM, thus suggesting that brain

atrophy may be relevant in determining the course of the disease and eventually disease progression. No differences were found in the small group of PP patients. So far, the intercorrelations between lesion load and WM and GM have been only partially addressed.

In 26 patients with MS, T1- and T2-weighted lesion volumes were inversely related to fGM but not to fWM (Chard, 2002). In 50 RR patients, faWM was inversely correlated to fGM but not to global fWM (Quarantelli, 2003). In patients with RR MS, a significant correlation between neocortical atrophy and T2 lesion volume was found, whereas no correlation was found in PP patients (De Stefano, 2003). We showed that lesion load is significantly correlated with both GM and WM atrophy; however, a significantly stronger relationship was found with fGM than with fWM. These results support the hypothesis that GM atrophy is heavily dependent on lesion load, possibly owing to retrograde degeneration of GM neurons secondary to fibers traversing WM lesions (Ge, 2001) (Bozzali, 2002), although we cannot ignore the possibility of both discrete and diffuse independent GM lesions that may be undetectable by conventional MRI (Peterson, 2001) (Kidd, 1999). Measurements of MRI-segmented volumes were significantly correlated to disability and age at disease onset and, to a lesser extent, drug treatment. So far, the studies addressing the relationship between MRI and disability have reported conflicting results, and this has been attributed to the poor sensitivity of the EDSS, although, more recently, functional MRI studies (Filippi and Rocca, 2003) suggested that the possible impact of plasticity may play a key role in determining the resulting disability. Significant correlations between disability and WM and GM atrophy were not found in 30 patients with RR MS

(Ge, 2001). A significant correlation between neocortical atrophy and EDSS was described in both RR and PP patients, whereas the correlation with disease duration was found only in RR patients (De Stefano, 2003). A significant correlation between GM atrophy and EDSS was reported, but there was no correlation between WM atrophy and disease duration (Chard, 2002). We produced very strong evidence that lesion load and both WM and GM atrophy are significantly correlated with disability. The existence of a close relationship between GM atrophy and disability is further supported by the significant association found in the analysis of predictors of disability. This correlation supports the role that GM involvement may play in the pathogenesis of MS and urges us to focus on neurodegeneration as a key feature of MS.

The correlation with age at disease onset suggests that the younger the age at disease onset, the worse the lesion load and brain atrophy (especially of WM) will be. These data suggest that brain atrophy is related to what happens at the very beginning of the disease rather than during the disease course. This hypothesis is in accordance with previous reports. Global brain atrophy (as derived from the parenchymal fraction) and central atrophy (as derived from the ventricular fraction) were longitudinally measured in 83 patients with MS at an interval of 2 to 4 years (Kalkers, 2002). The main observations were that clinical characteristics (such as duration of symptoms and ΔEDSS) did not predict the variance in the rate of global or central atrophy, whereas the rate of central atrophy was significantly higher in younger patients. Twenty-eight patients with MS were followed for up to 14 years after the first onset of symptoms (Chard, 2003), and lesion load in the first 5 years was more closely correlated with

disease-related brain atrophy at 14 years than were later changes in lesion load. Furthermore, in a cohort of patients with RR MS, lesion load (as derived from the average number of total and new gadolinium-enhanced lesions) decreased significantly with increasing patient age, independently of disease duration and relapse rate (Filippi, 2001). In line with the use of IFNβ in clinical practice, in a cross-sectional survey, it was found that patients assigned to treatment with IFNβ had a higher lesion load (adjusted mean of 1.6%; 95% CI 1.4 to 1.7) than those who had never received this drug because a watchful-waiting approach had been preferred (1.2%; 95% CI 1.0 to 1.5).

Regional findings: GM

Comparing our results to the only other work assessing cross-sectionally regional cortical GM loss in MS (Sailer, 2003), we are confirming a preferential fronto-temporal cortical atrophy, although in that paper the involvement of precentral cortex was appreciated only for patient subgroups with longer disease duration, more severe disability and larger LL, and did not appear to be lateralized. Furthermore, in our data there is a lack of correlation between cortical GM loss and EDSS, disease duration or LL.

Comparison of these results is however quite difficult for several reasons, including the use of different segmentation techniques (mono- vs. multiparametric), different measured entities (cortical thinning vs. local GM volume) and statistical analysis (ROI-based vs. voxel-based analysis when assessing correlations with clinical data), as well as different patient populations,

(mixed disease courses vs. pure RR MS), and further studies will be necessary to assess these differences.

In particular, monoparametric and multiparametric segmentation techniques may have different accuracies, especially in presence of MS lesions (whose effect was however specifically ruled out in our case), while the assessment of the cortical thinning and of changes in local GM volume has different localization capabilities (in principle in favor of the cortical thickness assessment, which includes a smoothing limited to the cortical surface, while VBM implies a full 3D smoothing).

Finally, the presence of progressive forms of MS in Sailer's patient population, as well as differences in the clinical severity of the patient groups in the two studies (in our case only RR MS patients with EDSS $\leq$ 4.5 were selected, compared to patients with mixed disease course and EDSS $\leq$ 7 in the paper by Sailer et al., may have played a major role.

Also a more recent study (Chen, 2004) assessing longitudinally the GM thickness in a mixed MS patient population (including both RR and secondary progressive disease course), has demonstrated a preferential correlation between the cortical thinning, especially in the precentral and parietal cortex, and the progression of disability over one year.

Again, the differences in patient population (in our case only RR MS patients were included) and methodology may well explain the different findings as compared to our study, where a consequential cross-sectional finding of correlation between disability and atrophy was not present.

Among the deep GM structures, caudate nuclei also presented a highly significant bilateral volume loss, correlating with LL.

Caudate nuclei border the lateral ventricles and may thus be prone to an indirect effect of ventricular enlargement due to spatial normalization inaccuracies, which may partly explain this finding. However, although the possibility that both mechanisms (true GM loss and normalization inaccuracies) are simultaneously present cannot be fully excluded, it should be reminded that caudate atrophy has been already detected in MS using manual parcellation (Bermel, 2003), although in that study no significant correlation with LL emerged.

The lateralization of the GM loss, especially at the level of the motor area and transverse temporal cortex, does not seem related to the location of the plaques that presented a symmetric distribution (Fig. 18).

To the best of our knowledge this is the first report of an asymmetric pattern of GM loss, with a preferential involvement of the left hemisphere in MS.

Previously, lateralized functional changes have been described in MS, in relationship to cognitive disturbances, including left fronto-temporal metabolic and CBF reductions (Pozzilli, 1991; Pozzilli 1992) with a preferential correlation to deficits in verbal fluency and verbal memory, and alterations of the P600 component of event related potentials in the left frontal and temporoparietal areas, in patients with memory disturbances (Sfagos, 2003).

Although studies of MRI correlates of cognitive impairment in MS have reported in most cases a correlation with LL (Blinkenberg, 2000; Camp, 1999; Hohol, 1997; Rao, 1989), this correlation appeared weak when were studied only RR-MS

patients (Fulton, 1999; Rovaris, 2002), a subgroup for which GM loss is emerging as a potential imaging correlate of cognitive impairment (Amato, 2004) .

From this perspective regional GM loss may contribute to clarify the pathogenesis of specific deficits such as those reported in MS for the paced auditory serial addition test, which activates preferentially left fronto-parieto-temporal areas (Audoin, 2005) or for tests of verbal fluency, more frequently altered in RR MS compared to progressive forms of the disease (Huijbregts, 2004). Preferential left atrophy may also partly contribute to previously described correlations between NAA loss in the left hemisphere and cognitive dysfunction in MS (Pan, 2001), a finding however not replicated in patients with more compromised verbal memory abilities with mixed disease course (Christodoulou, 2003).

These information on the spatial distributions of aWM and GM loss have implications in the assessment of the mechanisms potentially underlying cortical atrophy in multiple sclerosis.

Putative mechanisms for GM loss in MS include both Wallerian and retrograde neuroaxonal degeneration, which could partly contribute to the observed GM loss (Narayanan, 1997).

However, it should be considered that if neuroaxonal degeneration was the main driving force of GM loss, visual cortex atrophy would also be expected due to the extensive involvement of optic pathways which occurs frequently in MS, while our data document a relative sparing of occipital GM, in agreement with previous results using different segmentation and analysis technique (Sailer, 2003).

Another mechanism for GM damage is the possible direct inflammatory damage (Kidd, 1999), which is expected due to the frequency of juxtacortical MS lesions and to the presence of MS lesions within GM.

In particular, purely intracortical lesions represent up to 24% of the total LL (Kidd, 1999), and are particularly prominent in the frontal and the superior temporal lobe (Lumsden, 1970) and in the cingulate gyrus (Bo, 2003), with demyelination, axonal transection, dendritic transection, and apoptotic loss of neurons being detected at neuropathological studies (Peterson, 2001), although the mechanisms of tissue damage are still unclear, as cortical lesions show a different pattern of inflammation (fewer CD3-positive lymphocytes and CD68-positive microglia/macrophages than WM lesions) (Peterson, 2001).

However, to confirm the correlation between intracortical lesions and GM loss, the lateralization of GM loss that we found should be coupled to a lateralization of intracortical lesions, a finding, although not specifically assessed, not reported by previous studies.

Although visual assessment of the VBM results in subgroups of MS patients delineated an increased extent of the atrophic cortical areas with increasing LL, DD and EDSS, direct search for a correlation between these parameters and local GM volume did not show significant correlations for EDSS and DD while only limited cortical and subcortical clusters (caudates, motor cortex and hippocampus mainly) showed a correlation of atrophy with LL.

This is not surprising as it is expected an increase in the extension of the affected GM regions with advancing pathology, rather than an increase in the degree of atrophy in the same regions.

The selective correlation with LL of caudate, motor cortex and hippocampal atrophy may suggest a different mechanism of involvement of these regions compared to other cortical GM, possibly related to the accumulation of damage with disease progression. In particular for basal ganglia, which are interconnected to a larger number of areas of the brain through basal ganglia-thalamo-cortical circuits (Alexander and Crutcher, 1990), an increased sensitivity to damage deriving from remote axonal transection through anterograde and retrograde neuronal degeneration can be hypothesized, as opposed to other areas of the brain where GM loss may result from other mechanisms. From this perspective is somewhat more surprising that the same relationship (between atrophy and LL) was not found also for thalami, a structure whose structural damage, correlated to distant normal-appearing WM axonal loss, as demonstrated in RR-MS using diffusion tensor and MR spectroscopy (Wylezinska, 2003) (see discussion on WM results).

Finally, direct selective targeting and/or selective sensitivity of the affected regions to (as now unidentified) neurotoxic factors remains a viable hypothesis.

Regional findings: WM

Regional WM loss in MS has not been assessed at our knowledge. In previous studies assessing loss over pre-defined brain regions, decreases in both area and axonal density in corpus callosum (Evangelou, 2000) and in thalamic GM (Cifelli, 2002) have been reported.

Our VBM results on WM loss confirmed these findings showing a preferential location at the level of supratentorial periventricular regions, the involvement

being almost symmetrically distributed with a preferential involvement of the splenium of the corpus callosum.

Involvement of thalami deserves a specific attention as this finding was to be expected as a results of GM loss. Conventional MRI segmentation is probably not sufficiently accurate in assessing the thalami, which are composed by GM nuclei interspersed in WM tracts and consequently difficult to segment appropriately, even when taking advantage of multiple MR information simultaneously by the use of a multiparametric approach as in this case.

CONCLUSIONS

Our findings on quantification of GM and WM volumes in a large population of MS patients, confirmed both GM and global WM loss in patients as compared to normal subjects. Moreover MRI data showed significant differences between patients with relapsing–remitting and secondary progressive forms of MS: secondary progressive patients have significantly more atrophy of both WM and GM than do relapsing–remitting patients and a significantly higher lesion load. Significant correlations among MRI parameters and between MRI and clinical data were found. Lesion load correlates to both WM and even more to GM atrophy; lesion load and WM and GM atrophy are significantly related to Expanded Disability Status Scale score and age at onset (suggesting that the younger the age at disease onset, the worse the lesion load and brain atrophy); and GM atrophy is the most significant MRI variable in determining the final disability.

The two findings together confirm that a neurodegenerative phenomena should be considered.

Moreover in RR MS the loss of GM appears preferentially located in the left fronto-temporal cortex and precuneus, in the anterior cingulate gyrus, and bilaterally in caudate nuclei, while WM analysis showed preferential loss at the level of supratentorial periventricular regions and thalami.

The asymmetrical distribution of cortical atrophy is not explained by the volume of aWM or its symmetrical spatial distribution, and thus other mechanisms are probably involved in determining cortical GM loss, beside neuronal degeneration

from axonal transection in areas of the brain remote from GM, which probably plays a more direct role in deep GM atrophy.

Future work needed to assess whether the differences in MS subtypes are correlated to differences in regional brain tissue volumes.

BIBLIOGRAPHY

Adams, H.P., Koziol, J.A., 2000. Progressive cerebral atrophy in MS: a serial study using registered, volumetric MRI. Neurology 55, 1242-3.

Alexander, G.E., Crutcher, M.D., 1990. Functional architecture of basal ganglia circuits: neural substrates of parallel processing. Trends Neurosci 13, 266-71.

Alfano, B., Brunetti, A., Covelli, E.M., Quarantelli, M., Panico, M.R., Ciarmiello, A., et al., 1997. Unsupervised, automated segmentation of the normal brain using a multispectral relaxometric magnetic resonance approach. Magn Reson Med 37, 84-93.

Alfano, B., Brunetti, A., Larobina, M., Quarantelli, M., Tedeschi, E., Ciarmiello, A., et al., 2000. Automated segmentation and measurement of global white matter lesion volume in patients with multiple sclerosis. J Magn Reson Imaging 12, 799-807.

Alfano, B., Quarantelli, M., Brunetti, A., Larobina, M., Covelli, E.M., Tedeschi, E., et al., 1998. Reproducibility of intracranial volume measurement by unsupervised multispectral brain segmentation. Magn Reson Med 39, 497-9.

Amato, M.P., Bartolozzi, M.L., Zipoli, V., Portaccio, E., Mortilla, M., Guidi, L., et al., 2004. Neocortical volume decrease in relapsing-remitting MS patients with mild cognitive impairment. Neurology 63, 89-93.

Ashburner, J., Friston, K.J., 1999. Nonlinear spatial normalization using basis functions. Hum Brain Mapp 7, 254-66.

Ashburner, J., Friston, K.J., 2000. Voxel-based morphometry--the methods. Neuroimage 11, 805-21.

Ashburner, J., Neelin, P., Collins, D.L., Evans, A., Friston, K., 1997. Incorporating prior knowledge into image registration. Neuroimage 6, 344-52.

Atkins, M.S., Mackiewich, B.T., 1998. Fully automatic segmentation of the brain in MRI. IEEE Trans Med Imaging 17, 98-107.

Audoin, B., Ibarrola, D., Au Duong, M.V., Pelletier, J., Confort-Gouny, S., Malikova, I., et al., 2005. Functional MRI study of PASAT in normal subjects. Magma 18, 96-102.

Bakker, C.J., de Graaf, C.N., van Dijk, P., 1984. Derivation of quantitative information in NMR imaging: a phantom study. Phys Med Biol 29, 1511-25.

Bermel, R.A., Innus, M.D., Tjoa, C.W., Bakshi, R., 2003. Selective caudate atrophy in multiple sclerosis: a 3D MRI parcellation study. Neuroreport 14, 335-9.

Blinkenberg, M., Rune, K., Jensen, C.V., Ravnborg, M., Kyllingsbaek, S., Holm, S., et al., 2000. Cortical cerebral metabolism correlates with MRI lesion load and cognitive dysfunction in MS. Neurology 54, 558-64.

Bo, L., Vedeler, C.A., Nyland, H.I., Trapp, B.D., Mork, S.J., 2003. Subpial demyelination in the cerebral cortex of multiple sclerosis patients. J Neuropathol Exp Neurol 62, 723-32.

Bozzali, M., Cercignani, M., Sormani, M.P., Comi, G., Filippi, M., 2002. Quantification of brain gray matter damage in different MS phenotypes by use of diffusion tensor MR imaging. AJNR Am J Neuroradiol 23, 985-8.

Brummer, m., Mersereau, r., Eisner, r., Lewine, r., 1993. Automatic detection of brain contours in MRI data sets. IEEE Transactions on Medical imaging 12, 153-166.

Camp, S.J., Stevenson, V.L., Thompson, A.J., Miller, D.H., Borras, C., Auriacombe, S., et al., 1999. Cognitive function in primary progressive and transitional progressive multiple sclerosis: a controlled study with MRI correlates. Brain 122 (Pt 7), 1341-8.

Chakraborty, A., Staib, L., Duncan, J.S. An integrated approach to boundary finding in medical images. IEEE Workshop on Biomedical Image Analysis. Los Alamos, CA, 1994: 13-22.

Chard, D.T., Brex, P.A., Ciccarelli, O., Griffin, C.M., Parker, G.J., Dalton, C., et al., 2003. The longitudinal relation between brain lesion load and atrophy in multiple sclerosis: a 14 year follow up study. J Neurol Neurosurg Psychiatry 74, 1551-4.

Chard, D.T., Griffin, C.M., Parker, G.J., Kapoor, R., Thompson, A.J., Miller, D.H., 2002. Brain atrophy in clinically early relapsing-remitting multiple sclerosis. Brain 125, 327-37.

Chen, J.T., Narayanan, S., Collins, D.L., Smith, S.M., Matthews, P.M., Arnold, D.L., 2004. Relating neocortical pathology to disability progression in multiple sclerosis using MRI. Neuroimage 23, 1168-75.

Christodoulou, C., Krupp, L.B., Liang, Z., Huang, W., Melville, P., Roque, C., et al., 2003. Cognitive performance and MR markers of cerebral injury in cognitively impaired MS patients. Neurology 60, 1793-8.

Cifelli, A., Arridge, M., Jezzard, P., Esiri, M.M., Palace, J., Matthews, P.M., 2002. Thalamic neurodegeneration in multiple sclerosis. Ann Neurol 52, 650-3.

Dalton, C.M., Chard, D.T., Davies, G.R., Miszkiel, K.A., Altmann, D.R., Fernando, K., et al., 2004. Early development of multiple sclerosis is associated with progressive grey matter atrophy in patients presenting with clinically isolated syndromes. Brain 127, 1101-7.

Davie, C.A., Barker, G.J., Webb, S., Tofts, P.S., Thompson, A.J., Harding, A.E., et al., 1995. Persistent functional deficit in multiple sclerosis and autosomal dominant cerebellar ataxia is associated with axon loss. Brain 118 (Pt 6), 1583-92.

Davie, C.A., Hawkins, C.P., Barker, G.J., Brennan, A., Tofts, P.S., Miller, D.H., et al., 1994. Serial proton magnetic resonance spectroscopy in acute multiple sclerosis lesions. Brain 117 (Pt 1), 49-58.

Dawant, B.M., Hartmann, S.L., Thirion, J.P., Maes, F., Vandermeulen, D., Demaerel, P., 1999. Automatic 3-D segmentation of internal structures of the head in MR images using a combination of similarity and free-form transformations: Part I, Methodology and validation on normal subjects. IEEE Trans Med Imaging 18, 909-16.

De Stefano, N., Matthews, P.M., Filippi, M., Agosta, F., De Luca, M., Bartolozzi, M.L., et al., 2003. Evidence of early cortical atrophy in MS: relevance to white matter changes and disability. Neurology 60, 1157-62.

De Stefano, N., Narayanan, S., Francis, G.S., Arnaoutelis, R., Tartaglia, M.C., Antel, J.P., et al., 2001. Evidence of axonal damage in the early stages of multiple sclerosis and its relevance to disability. Arch Neurol 58, 65-70.

Edwards, S.G., Gong, Q.Y., Liu, C., Zvartau, M.E., Jaspan, T., Roberts, N., et al., 1999. Infratentorial atrophy on magnetic resonance imaging and disability in multiple sclerosis. Brain 122 (Pt 2), 291-301.

Evangelou, N., Konz, D., Esiri, M.M., Smith, S., Palace, J., Matthews, P.M., 2000. Regional axonal loss in the corpus callosum correlates with cerebral white matter lesion volume and distribution in multiple sclerosis. Brain 123 (Pt 9), 1845-9.

Farmer, M. Segmentation of Medical Images using Fuzzy CMeans Clustering, Oriented Edges, and a Recurrent Competitive Field Neural Network. University of Tennessee at Chattanooga, Department of Computer Science., 1996.

Ferguson, B., Matyszak, M.K., Esiri, M.M., Perry, V.H., 1997. Axonal damage in acute multiple sclerosis lesions. Brain 120 (Pt 3), 393-9.

Filippi, M., Rocca, M.A., 2003. Disturbed function and plasticity in multiple sclerosis as gleaned from functional magnetic resonance imaging. Curr Opin Neurol 16, 275-82.

Filippi, M., Wolinsky, J.S., Sormani, M.P., Comi, G., 2001. Enhancement frequency decreases with increasing age in relapsing-remitting multiple sclerosis. Neurology 56, 422-3.

Friston, K.J., Holmes, A.P., Poline, J.B., Grasby, P.J., Williams, S.C., Frackowiak, R.S., et al., 1995. Analysis of fMRI time-series revisited. Neuroimage 2, 45-53.

Fulton, J.C., Grossman, R.I., Udupa, J., Mannon, L.J., Grossman, M., Wei, L., et al., 1999. MR lesion load and cognitive function in patients with relapsing-remitting multiple sclerosis. AJNR Am J Neuroradiol 20, 1951-5.

Ge, Y., Grossman, R.I., Udupa, J.K., Babb, J.S., Nyul, L.G., Kolson, D.L., 2001. Brain atrophy in relapsing-remitting multiple sclerosis: fractional volumetric analysis of gray matter and white matter. Radiology 220, 606-10.

Good, C.D., Johnsrude, I., Ashburner, J., Henson, R.N., Friston, K.J., Frackowiak, R.S., 2001a. Cerebral asymmetry and the effects of sex and handedness on brain structure: a voxel-based morphometric analysis of 465 normal adult human brains. Neuroimage 14, 685-700.

Good, C.D., Johnsrude, I.S., Ashburner, J., Henson, R.N., Friston, K.J., Frackowiak, R.S., 2001b. A voxel-based morphometric study of ageing in 465 normal adult human brains. Neuroimage 14, 21-36.

Hartmann, S.L., Parks, M.H., Martin, P.R., Dawant, B.M., 1999. Automatic 3-D segmentation of internal structures of the head in MR images using a combination of similarity and free-form transformations: Part II, validation on severely atrophied brains. IEEE Trans Med Imaging 18, 917-26.

Hohol, M.J., Guttmann, C.R., Orav, J., Mackin, G.A., Kikinis, R., Khoury, S.J., et al., 1997. Serial neuropsychological assessment and magnetic resonance imaging analysis in multiple sclerosis. Arch Neurol 54, 1018-25.

Hojjatoleslami, S.A., Kruggel, F., 2001. Segmentation of large brain lesions. IEEE Trans Med Imaging 20, 666-9.

Holden, M., Steen, E., Lundervold, A., 1995. Segmentation and visualization of brain lesions in multispectral magnetic resonance images. Comput Med Imaging Graph 19, 171-83.

Huijbregts, S.C., Kalkers, N.F., de Sonneville, L.M., de Groot, V., Reuling, I.E., Polman, C.H., 2004. Differences in cognitive impairment of relapsing remitting, secondary, and primary progressive MS. Neurology 63, 335-9.

Jackson, E.F., Narayana, P.A., Wolinsky, J.S., Doyle, T.J., 1993. Accuracy and reproducibility in volumetric analysis of multiple sclerosis lesions. J Comput Assist Tomogr 17, 200-5.

Johnston, b., Atkins, M.S., Mackiewich, C., M, A., 1996. Segmentation of multiple sclerosis lesions in intensity corrected multispectral MRI. IEEE Transactions on Medical Imaging 15, 154-169.

Kalkers, N.F., Ameziane, N., Bot, J.C., Minneboo, A., Polman, C.H., Barkhof, F., 2002. Longitudinal brain volume measurement in multiple sclerosis: rate of brain atrophy is independent of the disease subtype. Arch Neurol 59, 1572-6.

Kamber, M., shingal, r., collins, d., Francis, G.S., evans, A., 1995. Model-based 3-D segmentation of multiple sclerosis lesions in magnetic resonance brain images. IEEE Transactions in Medical Imaging 14, 442-453.

Kapur, T. Segmentation of brain tissue from magnetic resonance images.: MIT AI Lab, 1995.

Karas, G.B., Burton, E.J., Rombouts, S.A., van Schijndel, R.A., O'Brien, J.T., Scheltens, P., et al., 2003. A comprehensive study of gray matter loss in patients with Alzheimer's disease using optimized voxel-based morphometry. Neuroimage 18, 895-907.

Kaus, M.R., Pekar, V., Lorenz, C., Truyen, R., Lobregt, S., Weese, J., 2003. Automated 3-D PDM construction from segmented images using deformable models. IEEE Trans Med Imaging 22, 1005-13.

Kidd, D., Barkhof, F., McConnell, R., Algra, P.R., Allen, I.V., Revesz, T., 1999. Cortical lesions in multiple sclerosis. Brain 122 (Pt 1), 17-26.

Kurtzke, J.F., 1983. Rating neurologic impairment in multiple sclerosis: an expanded disability status scale (EDSS). Neurology 33, 1444-52.

Laidlaw, D.H., Fleischer, K.W., Barr, A.H., 1998. Partial-volume Bayesian classification of material mixtures in MR volume data using voxel histograms. IEEE Trans Med Imaging 17, 74-86.

Letteboer, M.M., Olsen, O.F., Dam, E.B., Willems, P.W., Viergever, M.A., Niessen, W.J., 2004. Segmentation of tumors in magnetic resonance brain images using an interactive multiscale watershed algorithm. Acad Radiol 11, 1125-38.

Liu, C., Edwards, S., Gong, Q., Roberts, N., Blumhardt, L.D., 1999. Three dimensional MRI estimates of brain and spinal cord atrophy in multiple sclerosis. J Neurol Neurosurg Psychiatry 66, 323-30.

Losseff, N.A., Wang, L., Lai, H.M., Yoo, D.S., Gawne-Cain, M.L., McDonald, W.I., et al., 1996. Progressive cerebral atrophy in multiple sclerosis. A serial MRI study. Brain 119 (Pt 6), 2009-19.

Lublin, F.D., Reingold, S.C., 1996. Defining the clinical course of multiple sclerosis: results of an international survey. National Multiple Sclerosis

Society (USA) Advisory Committee on Clinical Trials of New Agents in Multiple Sclerosis. Neurology 46, 907-11.

Luders, E., Gaser, C., Jancke, L., Schlaug, G., 2004. A voxel-based approach to gray matter asymmetries. Neuroimage 22, 656-64.

Lumsden, C. The neuropathology of multiple sclerosis. In: Vinken PJ BG, editor. Handbook of clinical neurology. Vol 9. Amsterdam: North-Holland, 1970: 217-309.

McDonald, W.I., Compston, A., Edan, G., Goodkin, D., Hartung, H.P., Lublin, F.D., et al., 2001. Recommended diagnostic criteria for multiple sclerosis: guidelines from the International Panel on the diagnosis of multiple sclerosis. Ann Neurol 50, 121-7.

Miller, D.H., Barkhof, F., Frank, J.A., Parker, G.J., Thompson, A.J., 2002. Measurement of atrophy in multiple sclerosis: pathological basis, methodological aspects and clinical relevance. Brain 125, 1676-95.

Mitchell, J.R., Karlik, S.J., Lee, D.H., Fenster, A., 1994. Computer-assisted identification and quantification of multiple sclerosis lesions in MR imaging volumes in the brain. J Magn Reson Imaging 4, 197-208.

Mohamed, F.B., Vinitski, S., Faro, S.H., Gonzalez, C.F., Mack, J., Iwanaga, T., 1999. Optimization of tissue segmentation of brain MR images based on multispectral 3D feature maps. Magn Reson Imaging 17, 403-9.

Narayanan, S., Fu, L., Pioro, E., De Stefano, N., Collins, D.L., Francis, G.S., et al., 1997. Imaging of axonal damage in multiple sclerosis: spatial distribution of magnetic resonance imaging lesions. Ann Neurol 41, 385-91.

Pan, J.W., Krupp, L.B., Elkins, L.E., Coyle, P.K., 2001. Cognitive dysfunction lateralizes with NAA in multiple sclerosis. Appl Neuropsychol 8, 155-60.

Pannizzo, F., Stallmeyer, M.J., Friedman, J., Jennis, R.J., Zabriskie, J., Plank, C., et al., 1992. Quantitative MRI studies for assessment of multiple sclerosis. Magn Reson Med 24, 90-9.

Pelletier, D., Garrison, K., Henry, R., 2004. Measurement of whole-brain atrophy in multiple sclerosis. J Neuroimaging 14, 11S-19S.

Peterson, J.W., Bo, L., Mork, S., Chang, A., Trapp, B.D., 2001. Transected neurites, apoptotic neurons, and reduced inflammation in cortical multiple sclerosis lesions. Ann Neurol 50, 389-400.

Poser, C.M., Paty, D.W., Scheinberg, L., McDonald, W.I., Davis, F.A., Ebers, G.C., et al., 1983. New diagnostic criteria for multiple sclerosis: guidelines for research protocols. Ann Neurol 13, 227-31.

Quarantelli, M., Ciarmiello, A., Morra, V.B., Orefice, G., Larobina, M., Lanzillo, R., et al., 2003. Brain tissue volume changes in relapsing-remitting multiple sclerosis: correlation with lesion load. Neuroimage 18, 360-6.

Ranganath, s., 1995. Contour extraction from cardiac MRI studies using snake. IEEE Transactions on Medical imaging 14, 328-338.

Rao, S.M., Leo, G.J., Haughton, V.M., St Aubin-Faubert, P., Bernardin, L., 1989. Correlation of magnetic resonance imaging with neuropsychological testing in multiple sclerosis. Neurology 39, 161-6.

Rooney, W.D., Goodkin, D.E., Schuff, N., Meyerhoff, D.J., Norman, D., Weiner, M.W., 1997. 1H MRSI of normal appearing white matter in multiple sclerosis. Mult Scler 3, 231-7.

Rovaris, M., Iannucci, G., Falautano, M., Possa, F., Martinelli, V., Comi, G., et al., 2002. Cognitive dysfunction in patients with mildly disabling relapsing-remitting multiple sclerosis: an exploratory study with diffusion tensor MR imaging. J Neurol Sci 195, 103-9.

Rudick, R.A., Fisher, E., Lee, J.C., Simon, J., Jacobs, L., 1999. Use of the brain parenchymal fraction to measure whole brain atrophy in relapsing-remitting MS. Multiple Sclerosis Collaborative Research Group. Neurology 53, 1698-704.

Sailer, M., Fischl, B., Salat, D., Tempelmann, C., Schonfeld, M.A., Busa, E., et al., 2003. Focal thinning of the cerebral cortex in multiple sclerosis. Brain 126, 1734-44.

Sfagos, C., Papageorgiou, C.C., Kosma, K.K., Kodopadelis, E., Uzunoglu, N.K., Vassilopoulos, D., et al., 2003. Working memory deficits in multiple sclerosis: a controlled study with auditory P600 correlates. J Neurol Neurosurg Psychiatry 74, 1231-5.

Simon, J.H., Jacobs, L.D., Campion, M.K., Rudick, R.A., Cookfair, D.L., Herndon, R.M., et al., 1999. A longitudinal study of brain atrophy in relapsing multiple sclerosis. The Multiple Sclerosis Collaborative Research Group (MSCRG). Neurology 53, 139-48.

Suzuki, H., Toriwaki, J., 1991. Automatic segmentation of head MRI images by knowledge guided thresholding. Comput Med Imaging Graph 15, 233-40.

Talairach, J., Tournoux, P. Co-planar Stereotaxic Atlas of the Human Brain - 3-Dimensional Proportional system: An Approach to cerebral imaging. New york: Thieme, 1988.

Trapp, B.D., Peterson, J., Ransohoff, R.M., Rudick, R., Mork, S., Bo, L., 1998. Axonal transection in the lesions of multiple sclerosis. N Engl J Med 338, 278-85.

Udupa, J.K., Wei, L., Samarasekera, S., Miki, Y., van Buchem, M.A., Grossman, R.I., 1997. Multiple sclerosis lesion quantification using fuzzy-connectedness principles. IEEE Trans Med Imaging 16, 598-609.

Vaillant, M., Davatzikos, C., 1997. Finding parametric representations of the cortical sulci using an active contour model. Med Image Anal 1, 295-315.

Van Leemput, K., Maes, F., Vandermeulen, D., Colchester, A., Suetens, P., 2001. Automated segmentation of multiple sclerosis lesions by model outlier detection. IEEE Trans Med Imaging 20, 677-88.

Woods, R.P., Grafton, S.T., Watson, J.D., Sicotte, N.L., Mazziotta, J.C., 1998. Automated image registration: II. Intersubject validation of linear and nonlinear models. J Comput Assist Tomogr 22, 153-65.

Wylezinska, M., Cifelli, A., Jezzard, P., Palace, J., Alecci, M., Matthews, P.M., 2003. Thalamic neurodegeneration in relapsing-remitting multiple sclerosis. Neurology 60, 1949-54.

Zijdenbos, A.P., Dawant, b., Margolin, r., Palmer, a., 1994. Morphometric analysis of white matter lesions in MR images: method and validation. IEEE Transactions on Medical Imaging 13, 716-724.